Electrochimica Acta 514 (2025) 145620

Contents lists available at ScienceDirect

Electrochimica Acta

journal homepage: www.journals.elsevier.com/electrochimica-acta

Binary transition metal and ZIF-8 functionalised polymer-derived ceramic catalysts for high temperature PEM fuel cell cathode

Marek Mooste [a,b,*], Julia Müller-Hülstede [a], Dana Schonvogel [a], Tanja Zierdt [a], Julia Buschermöhle [a], Killian Fuhrmann [a], Michaela Wilhelm [c], Peter Wagner [a], K. Andreas Friedrich [d]

[a] Institute of Engineering Thermodynamics, German Aerospace Center (DLR), Carl-von-Ossietzky-Str. 15, 26129 Oldenburg, Germany
[b] Institute of Chemistry, University of Tartu, Ravila 14a, 50411 Tartu, Estonia
[c] Advanced Ceramics, University of Bremen, Am Biologischen Garten 2, IW3, 28359 Bremen, Germany
[d] Institute of Engineering Thermodynamics, German Aerospace Center (DLR), Pfaffenwaldring 38-40, 70569 Stuttgart, Germany

ARTICLE INFO

Keywords:
Electrocatalysis
Oxygen reduction reaction
Non-precious metal catalyst
High-temperature PEMFC
Dual-atom catalysts
ZIF-8

ABSTRACT

For addressing the clean energy transition, the high-temperature proton exchange membrane fuel cells (HT-PEMFC) are attractive energy conversion devices for the long-range and heavy-duty vehicles, auxiliary power units, and aviation applications. One current drawback inhibiting HT-PEMFC commercialisation is the need for non-precious metal catalyst (NPMC) for oxygen reduction reaction (ORR) at the cathode. Here we propose the polymer derived ceramics (PDC) based material silicon oxycarbide (SiOC) with double transition metal (TM) doping and N-functionalisation for the NPMC preparation. The catalysts prepared with zeolitic imidazolate framework-8 (ZIF-8) as a N source exhibited high specific surface area, hierarchical porosity, and presence of TM (alloy) nanoparticles together with atomically dispersed TMs. The highest activity towards the ORR was observed in the case of Fe/Co containing and acid leached catalyst material (CoFe-N-SiOCa) exhibiting the highest long-term durability in 0.5 M H_3PO_4 solution and the best performance during the GDE testing in conc. H_3PO_4 at 160 °C. During HT-PEMFC testing, the open circuit voltage of 768 mV and power density at 100 mA cm^{-2} of 34 mW cm^{-2} with CoFe-N-SiOCa cathode were registered.

1. Introduction

The high-temperature proton exchange membrane fuel cells (HT-PEMFC) are an alternative to already commercially available low-temperature PEMFC technology to address the growing global need for renewable energy conversion devices [1,2]. For example, the favourable benefits of HT-PEMFC are the possibility to use lower purity hydrogen fuels (e.g., reformate hydrogen from methanol), simplified water management, and enhanced electrochemical kinetics as well as more efficient cooling due to high temperature [1,3,4]. One major issue for implementing the HT-PEMFC devices is the need for non-precious metal catalysts (NPMC) at the cathode to replace the easily poisoned and expensive Pt-based oxygen reduction reaction (ORR) catalyst (Pt/C) [5,6]. The ORR in acidic medium can proceed via two alternative pathways, direct $4e^-$ pathway, Eq. (1) [6,7],

$$O_2 + 4e^- + 4H^+ \rightarrow 2H_2O, \quad (1)$$

or $2e^-$ reduction, which is less favoured for PEMFC application, Eq. (2),

$$O_2 + 2e^- + 2H^+ \rightarrow H_2O_2, \quad (2)$$

the H_2O_2 can proceed further $2e^-$ reduction, Eq. (3) resulting in $2\times2e^-$ pathway,

$$H_2O_2 + 2e^- + 2H^+ \rightarrow 2H_2O. \quad (3)$$

In the PEMFC conditions, the direct $4e^-$ and $2 \times 2e^-$ pathways are favourable and the TM and N co-doped high surface area nanocarbon materials are currently the most promising NPMC technologies [5,8,9].

The main challenges for NPMCs are the need for high ORR activity and long-term durability, which should be addressed simultaneously to obtain a catalyst with the potential for practical application [8,10]. Previously, the iron-nitrogen-carbon (Fe-N-C) material was experimentally shown to be the most active material for ORR in acidic electrolytes [11–13], primarily due to the atomic $Fe-N_4$ moieties. More recently,

* Corresponding author.
E-mail addresses: marek.mooste@dlr.de, marek.mooste@ut.ee (M. Mooste).

https://doi.org/10.1016/j.electacta.2024.145620
Received 23 September 2024; Received in revised form 17 December 2024; Accepted 30 December 2024
Available online 31 December 2024

researchers have directed the focus on bimetallic or multi-metallic (atomically dispersed) catalysts to further increase the ORR activity and catalyst durability (e.g., avoiding Fenton reactions due to the Fe^{2+}, decrease active site degradation rate) [14–16]. The transition metal (TM) activity order for ORR in acidic conditions has been reported to be Fe > Co > Mn > Cu > Ni [17]. There is no information available for the ORR activity comparison for these TM combinations (Fe/Co, Fe/Mn, Fe/Cu) and especially in the harsh HT-PEMFC conditions (conc. H_3PO_4 at 160 °C) [1,2].

The harsh HT-PEMFC conditions result also in another topical issue, which is chemical stability and durability of the nanocarbon catalyst support material [10,17]. Mainly due to the carbon corrosion, the development of extremely robust catalytic supports to withstand high temperatures is needed [8,18–20]. One attractive material for this application would be polymer derived ceramics (PDC) and especially it`s subclass silicon oxycarbide (SiOC), which have high thermal and chemical stability, and superior oxidation/corrosion resistance under harsh conditions [21]. Furthermore, the SiOC-based catalysts have been previously found to be suitable for alkaline environment fuel cell and battery applications and shown very good durability [22–25]. In one of the latter investigations, the N source dicyandiamide (DCDA) was used for the N-functionalisation, which also showed promising results for the ORR in acidic environment [25]. In more recent investigations, the zeolitic imidazolate framework-8 (ZIF-8) [26] has found very intensive use for N-doping and especially for the preparation of binary TM containing NPMC [27–35]. It has been reported that the ORR-inert Zn atoms in ZIF-8 effectively restrict the aggregation of TM atoms into nanoparticles during high-temperature pyrolysis, while also supporting the formation of micropores through volatilization, resulting in enhanced ORR activity [36–38].

In the present investigation, the double transition metal and N co-doped PDC-based electrocatalysts for HT-PEMFC cathode were prepared via pyrolysis. Three metal combinations (Fe/Cu, Fe/Mn, Fe/Co) were investigated together with two different N sources, ZIF-8 and DCDA. The pristine and acid leached [30,39] catalysts were subjected to physical characterisation and ORR half-cell studies in hydrodynamic conditions (0.5 H_3PO_4) and at gas diffusion electrode experiments (conc. H_3PO_4 at 160 °C). Finally, the most promising material was investigated at the HT-PEMFC cathode.

2. Experimental

2.1. Material preparation

The procedure for preparing binary TM-containing PDC-based ceramic catalysts precursor materials was based on our previous investigation [25] with several new modifications. To prepare the PDC material, the powders of poly(methyl phenyl silsesquioxane) (H44, Wacker Chemie AG), silicon resin poly(methylsilsesquioxane) (MK, Wacker Chemie AG), graphite (IMERYL Graphite & Carbon), azodicarboxamide (Azo, Sigma-Aldrich), and (3-Aminopropyl)triethoxysilane (APTES) were dissolved/dispersed in xylene (Sigma-Aldrich) under constant stirring at room temperature and a cross-linking was initiated via the addition of the imidazole (Imi, Alfa Aesar) and stirring for 20 min. For the preparation of double TM-containing PDC samples, the corresponding TM salts were included into the mixture of the powders prior to the cross-linking step. The used TM salts were copper(II) 2, 4-pentanedionate (CuAc, 98 %, abcr GmbH), iron(II) acetylacetonate (FeAc, 95 %, abcr GmbH), manganese(II) acetylacetonate (MnAc, Sigma Aldrich), cobalt(II) acetylacetonate (CoAc, Sigma Aldrich). The specific amounts of used precursor materials are given in Table 1.

The dried mixture of reagents was subjected to pyrolysis under a N_2 atmosphere using 2 °C min^{-1} up to 900 °C, 0.5 °C min^{-1} from 900 to 1000 °C, and kept at final temperature for 4 h. After that the material was cooled to a room temperature at a rate of 2 °C min^{-1}. The materials were further crushed manually and ball-milled (PM 400, Retsch) at 350 rpm min^{-1} for 4 h to produce a fine powder. The fine powder was sieved to particle sizes <100 μm and only this fraction was used for the catalyst preparation. These materials are denoted by the pair of transition metals used, followed by "PDC" (Table 1).

The N-functionalisation of the four different PDC materials (Table 1) was performed using the zeolitic imidazolate framework-8 (ZIF-8, Basolite® Z1200, Sigma-Aldrich) as a nitrogen source [31,32]. In brief, 1:1 weight ratio of PDC:ZIF-8 mixture was dispersed in methanol (99.9 %, Thermo Scientific Chemicals) via ultrasonication during 2 hours followed by the evaporation of the solvent at 60 °C overnight. The dry mixture was pyrolysed in N_2 environment using the tube furnace with a ceramic tube (RHTC 80-230/15, Nabertherm) and heating rate of 5 °C min^{-1} until 950 °C and followed by the dwelling time of 1 h at 950 °C. The obtained materials have -N-SiOC in their designation instead of PDC, e.g., CoFe-PDC-based catalyst is named as CoFe-N-SiOC after ZIF-8 modification. For the optimisation purposes of the catalyst preparation route, different PDC:ZIF-8 weight ratios and final pyrolysis temperatures between 900 and 1000 °C were also investigated. Furthermore, the 16-hour acid leaching procedures at 90 °C in 2 M H_2SO_4 (96 %, Merck) [39,40] or 3 M H_2SO_4 + HNO_3 (65 %, Carl Roth) mixture [41] were also employed, whereby the letters a or b, respectively, were appended to the name of the catalyst material.

For comparison purposes, the dicyandiamide (DCDA, 99 %, Sigma-Aldrich) route was also used for the N-functionalisation. The procedure itself was identical to the ZIF-8 route, except the PDC:DCDA weight ratios of 1:10, 1:20 [25] and pyrolysis temperatures of 800 [25] and 900 °C were used in the optimization of catalyst preparation. The obtained materials have additional -N in their designation, e.g., CoFe-PDC-based catalyst is named as CoFe-PDC-N after DCDA modification.

2.2. Physical characterization

For high resolution transmission electron microscopy (HR-TEM), a catalyst suspension in ethanol was applied to a 200-mesh copper grid coated with polyvinyl formal (Plano). Imaging was carried out using JEM-2100F (Jeol) coupled with an energy-dispersive X-ray spectrometer (EDS) at 200 kV accelerating voltage and AZTec software with a 250 X-Max80 SDD detector from Oxford Instruments.

For X-ray photoelectron spectroscopy (XPS) analyses an ESCALAB 250Xi (Thermo Fisher) was used with monochromatic Al-K_α radiation and a beam diameter of 650 μm. Three survey scans were recorded, using a transit energy of 100 eV, a dwell time of 20 ms and a step size of 1 eV. Furthermore, high-resolution X-ray photoelectron (XP) spectra for the elements C (1s, 4 scans), O (1 s, 8 scans), N (1 s, 10 scans), Si (2 p, 10 scans), Fe (2 p, 20 scans), Co (2 p, 10 scans), Cu (2 p, 20 scans), Mn (2 p, 20 scans) and Zn (2 p, 3 scans) were recorded. A transit energy of 20 eV, a dwell time of 50 ms and a step size of 0.02 eV were used. The Avantage software (Thermo Fisher) was used with smart background and Gauss-

Table 1
Composition of the powders used for the PDC-based electrocatalyst precursor solution preparation in xylene (wt%).

Catalyst	H44	MK	Graphite	Azo	Imi	TM salt 1	TM salt 2	APTES
PDC	12.8	12.8	33.7	19.6	1.1	0	0	20
CoFe-PDC	10.7	10.7	30	17.6	1	5 (FeAc)	5 (CoAc)	20
MnFe-PDC	10.7	10.7	30	17.6	1	5 (FeAc)	5 (MnAc)	20
CuFe-PDC	10.7	10.7	30	17.6	1	5 (FeAc)	5 (CuAc)	20

Lorentz line shape for peak fitting.

For the scanning electron microscopy with energy dispersive X-ray spectroscopy (SEM-EDS) analysis, the sample powders were sputtered with gold for 48 seconds using the sputtering machine Sputter Coater 108 Auto (Cressington). The SEM measurements were performed with SUPRA 40 (Zeiss) equipped with SE2 detector for the images, and the XFlash 6|30 (Bruker) detector for EDS. The X-ray diffraction (XRD) analysis were performed using the X-ray diffractometer (Seifert C 3000 Diffractometer MZ IV ISO, Germany) with Cu-K_α radiation. Nitrogen adsorption isotherms at 77 K were recorded and analysed (Belsorp-Mini, Bel Japan Inc.) to evaluate the specific surface area (SSA), calculated according to Brunauer-Emmett-Teller (BET) method [42]. Samples were measured as powder (particle size < 300 μm) and pre-conditioned prior to the measurements at 200 °C for 24 h under vacuum to remove water and gas molecules adsorbed on the surface of the materials.

2.3. RRDE and GDE half-cell studies

The rotating ring-disc electrode (RRDE) half-cell studies for ORR were performed in 0.5 M H_3PO_4 and 0.5 M H_2SO_4 solutions and the experimental details [25,43] for the RRDE measurements are given in the Supporting information (Section S1).

The gas diffusion electrode (GDE) half-cell measurements were performed with the similar setup and testing conditions as applied in an earlier report by Zierdt et al. for Fe-N-C (PMF-014401) catalyst investigation [44] with the exception of simplified catalyst ink deposition method [45,46]. The ink was prepared with 10 mg NPMC dispersed in 776 μl 2-propanol, 234 μl Milli-Q water, and 7.5 μl polytetrafluorethylene (PTFE, 60 %, Sigma-Aldrich) solution and sonicated for 1.5 h. The previously optimised NPMC/PTFE wt. ratio of 60/40 was used [44]. The ink was drop-cast onto a 3.33 cm^2 gas diffusion layer (GDL, Freudenberg H23C2) by 100 μl aliquots and left to dry at 60 °C between the coatings [46]. The GDE with the final NPMC loading of 3 mg cm^{-2} was hot pressed (TRG-2, P/O/Weber) with 1.5kN for 40s at 140 °C with a phosphoric-acid doped polybenzimidazole membrane (PA-PBI, Celtec®-P, TRIGONA Fuel Cell Components GmbH). The PA-PBI membrane was soaked 24 hours in 50 % H_3PO_4 prior to pressing and the stainless-steel shim shields with 80 % of total thickness were used to prevent over crushing of PA-PBI/GDE assembly. Afterwards, the PA-PBI/GDE assembly was sandwiched between the copper plate current collector and PTFE shield, which limited the geometric active area to 0.5 cm^2 for PA-PBI/GDE working electrode to be in contact with the electrolyte on the PA-PBI side and also 0.5 cm^2 for the O_2/N_2 breathing GDE side. The half-cell measurements were performed at 160 °C in a commercial FlexCell® PTFE (Gaskatel) setup with silicone gaskets using 40 mL of 85 % H_3PO_4, electrolyte, Pt coil counter electrode, and commercial RHE (Gaskatel) reference electrode [44]. The experiments were controlled using the potentiostat Modulab 2100A (Ametek) equipped with a 12V/20A external booster (Ametek) and the measurement protocol for half-cell experiments was adapted from Ehelebe et al [44,47]. Briefly, the protocol contained (i) "begin of test" (BoT) and (iii) "end of test" (EoT) cyclic voltammograms (CVs) with N_2 flow at the GDE and (ii) fixed time galvanostatic steps followed by electrochemical impedance spectroscopy (EIS) measurements for different polarisation currents with O_2 flow at the GDE, which was performed in-between the (i) BoT and (iii) EoT steps. The EIS data was used to calculate and apply iR-drop correction (95 %) for the recorded potentials at each galvanostatically applied current value ($E_{iR\_corrected} = E_{uncompensated} - I \times R$) [44].

2.4. HT-PEMFC measurements

The membrane electrode assembly (MEA) preparation and HT-PEMFC testing was performed according to the already published procedure [10]. The cathode fabrication and membrane treatment were similar to the GDE half-cell testing (Section 2.3). A commercial Pt/C anode (1 mg_{Pt} cm^{-2}, De Nora) was employed. Two cathodes with different catalysts, Fe-N-C (PMF-014401) and CoFe-N-SiOCa were investigated with each having a gravimetric loading of 3 ± 0.1 mg cm^{-2}. The PA-PBI membrane outlined to the active area of 4.05 cm^2 with Kapton® frames was sandwiched with cathode and anode using hot press with 1.0 kN for 30 s at 140 °C. After hot-pressing, a thermal annealing at 160 °C for 30 min was carried out in an air atmosphere. HT-PEMFC performance was evaluated using an HT-PEM single cell test station from Inhouse Engineering equipped with a quickCONNECTfixture (qCF 5/100 HT, balticFuelCells). A cell fixture cF5/100 HT Gr V1.4 with serpentine graphitic flow fields (balticFuelCells) was used with a cell compression of 0.75 MPa during the testing. After the gas non-leakage proof test, the cell temperature was ramped to 120 °C in N_2 flow. As a next step, gases were switched to dry H_2/O_2 with stoichiometry of 1.5/9.5 and the temperature was further ramped to 160 °C under a constant load of 100 mA cm^{-2}. After reaching 160 °C and the cell voltage stabilisation, a galvanostatic *U-I* polarization curve was recorded with a step size of 0.1 A until a minimal voltage of 0.1 V. Next, electrochemical impedance spectroscopy (EIS) was carried out at fixed current densities of 0.03, 0.1 A and 0.3 A cm^{-2} with equilibration time of 5 min each, an amplitude of 10 mV r.m.s. and a frequency range of 100 kHz to 100 mHz was used. For the CV testing, the N_2 flow rate of 0.1 L min^{-1} at the cathode and a H_2 flow rate of 0.1 L min^{-1} at the anode were applied with a scan rate of 100 mV s^{-1} in a range of 0.05-1.00 V. An external potentiostat Modulab2100A (Ametek) equipped with an external booster (12 V/20 A) was used for the EIS and CV measurements.

3. Results and discussion

3.1. Physical characterisation of the catalysts

The SEM-EDS experiments were performed to investigate the catalyst structure and composition on the micrometre scale (Fig. 1, Table 2). All the PDC catalyst powders were sieved to particle sizes <100 μm prior to use, which is also confirmed by SEM images as no agglomerates/particles above this size are observed. Very rough and disordered structures of the particles can be seen, which is consistent with our previous study of PDC materials [25] and indicates the high specific surface area of the material, which may harbour a large number of active sites for ORR. Interestingly, the surface structure and agglomerate/particle sizes of PDC materials prepared herein are very similar to the one of commercial Fe-N-C (Fig. 1e). The functionalisation with ZIF-8 has no observable effect on the ca. 100 × 100 μm area image on PDC materials as expected due to the ca. 0.1-0.2 μm dimensions of ZIF-8 particles. The EDS measurements showed the bulk composition of PDC catalysts to be rather uniform containing roughly around 75, 3, 13, and 5 at% of C, N, O, and Si elements, respectively. The N in PDC materials derives from the precursors of Azo, Imi, and APTES (Table 1). In the case of binary TM doped PDC catalysts, ca. 0.2-0.3 at% of each TM is observed, which is very similar to our previous investigation with single TM containing PDCs [25]. The effect of ZIF-8 modification is observed to increase the N content ca. two-fold and introduce ca. 0.3 at% of Zn despite the high pyrolysis temperature of 950 °C exceeding the one of Zn boiling point (907 °C). The latter TM itself is known to be rather inactive additive for ORR and its removal could be complicated [36]. Therefore, we preferred to retain it and take into consideration its potential influence. The observed two-fold increase in the N content could provide the significant increase in the number of N-based active sites for ORR. For comparison, the at% of Fe is twice as high and at% of N ca. 30 % larger in the case of all ZIF-8 functionalised catalysts (-N-SiOC) compared to the commercial Fe-N-C.

Nitrogen adsorption/desorption measurements were performed to study the specific surface area and mean pore diameter (d_p) of the PDC, N-SiOC materials and to compare these values with the state-of-the-art Fe-N-C catalyst (Fig. 2, Table 3). The isotherms of all the catalysts prepared in this work (Fig. 2a) have a similar shape and can be classified as type IV isotherms according to IUPAC showing a very distinct hysteresis

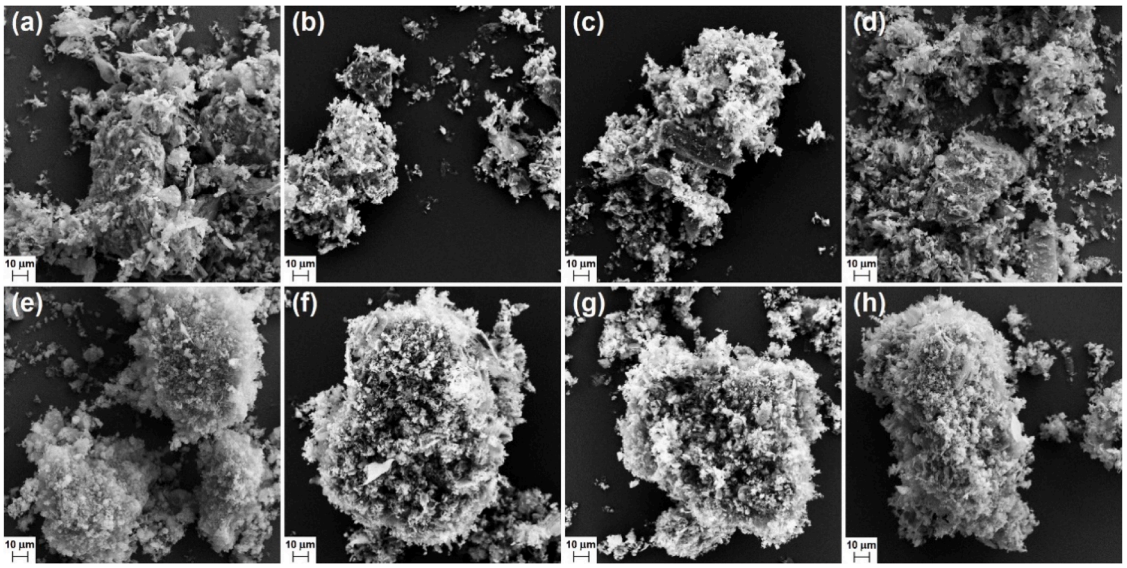

Fig. 1. SEM images of unmodified (a) PDC, (b) CoFe-PDC, (c) MnFe-PDC, (d) CuFe-PDC, (e) Fe-N-C (PMF-014401) and ZIF-8 functionalised materials (f) CoFe-N-SiOC, (g) MnFe-N-SiOC, (h) CuFe-N-SiOC.

Table 2
Elemental composition (at%) determined from EDS analysis for the Fe-N-C (PMF-014401), different PDC and ZIF-8 functionalised (-N-SiOC) materials.

	PDC	CoFe-PDC	CoFe-N-SiOC	MnFe-PDC	MnFe-N-SiOC	CuFe-PDC	CuFe-N-SiOC	Fe-N-C
C	73.7 ± 1.9	77.1 ± 3.5	75.5 ± 0.9	76.9 ± 1.0	78.4 ± 1.5	74.6 ± 7.4	76.8 ± 2.4	88.7 ± 0.3
N	2.70 ± 0.13	3.38 ± 0.13	6.30 ± 0.42	3.61 ± 0.28	6.71 ± 1.03	2.77 ± 1.26	7.34 ± 0.71	5.30 ± 0.20
O	18.3 ± 1.5	15.1 ± 2.4	13.3 ± 1.3	13.2 ± 0.7	10.3 ± 0.8	16.5 ± 4.8	12.1 ± 1.2	5.89 ± 0.30
Si	5.36 ± 0.67	4.04 ± 0.77	4.14 ± 0.62	5.65 ± 0.89	3.85 ± 0.35	4.78 ± 1.19	2.81 ± 1.49	-
Fe	-	0.21 ± 0.08	0.23 ± 0.05	0.35 ± 0.07	0.26 ± 0.04	0.25 ± 0.06	0.21 ± 0.06	0.12 ± 0.02
Mn	-	-	-	0.29 ± 0.06	0.20 ± 0.06	-	-	-
Co	-	0.20 ± 0.06	0.20 ± 0.07	-	-	-	-	-
Cu	-	-	-	-	-	0.26 ± 0.12	0.38 ± 0.13	-
Zn	-	-	0.29 ± 0.10	-	0.28 ± 0.15	-	0.28 ± 0.14	-

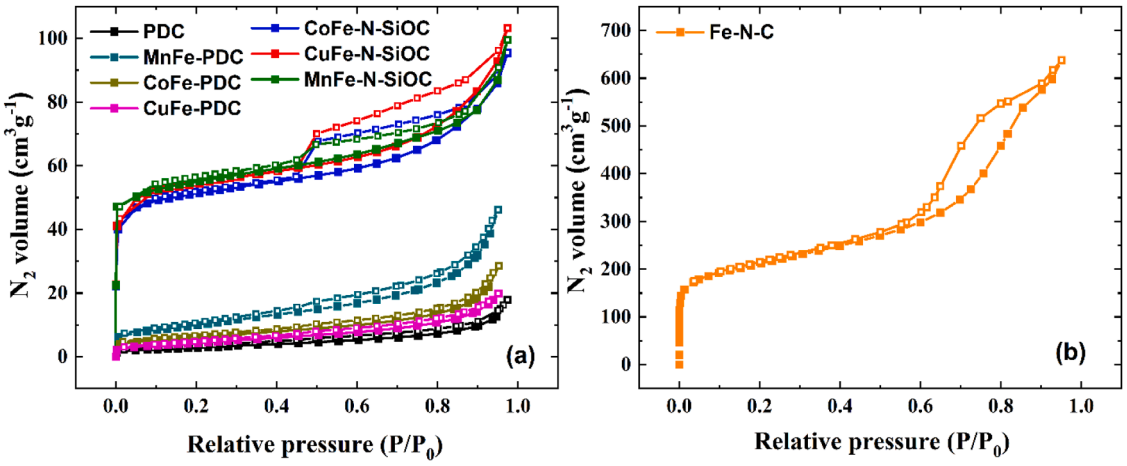

Fig. 2. N_2 adsorption-desorption isotherms for different (a) PDC and the ZIF-8 modified materials (-N-SiOC), (b) commercial Fe-N-C (PMF-014401) catalyst. Adsorption (■), desorption (□) measurement points.

loop of the form H2 [48]. The pore size distribution (data not shown) indicated that PDC and N-SiOC materials have hierarchical porosity containing both micro- and mesopores.

The isotherm of Fe-N-C material shows a characteristic hysteresis loop (Fig. 2b) exhibiting characteristic features of types H4 or H2b [49], indicating that the mesoporous carbon is consistent with the observed pore size distribution (data not shown). Mesoporosity of catalyst material is considered beneficial to enhance mass-transfer of O_2 molecules to the ORR active sites [50]. The BET surface area (S_{BET}) and d_p values for all PDC materials are in the range of ca. 10-34 $m^2\ g^{-1}$ and ca. 8-10 nm, respectively, which is in good agreement with our previous investigation of single TM containing PDC catalysts [25]. The functionalisation of double TM containing PDC materials with ZIF-8 results in the considerable growth of S_{BET} values to ca. 130-140 $m^2\ g^{-1}$ and the

Table 3
Textural properties for different catalyst materials shown in Fig. 2, monolayer volume (V_m, $cm^3\ g^{-1}$). BET surface area (S_{BET}, $m^2\ g^{-1}$), total pore volume (V_{tot}, $cm^3\ g^{-1}$) and mean pore diameter (d_p, nm).

	PDC	CoFe-PDC	CoFe-N-SiOC	MnFe-PDC	MnFe-N-SiOC	CuFe-PDC	CuFe-N-SiOC	Fe-N-C
V_m	2.5	4.7	30.3	7.9	32.6	3.7	32.1	137.3
S_{BET}	10.7	20.6	132.0	34.5	141.9	15.9	139.7	597.7
V_{tot}	0.03	0.04	0.15	0.07	0.15	0.03	0.16	0.99
d_p	10.4	8.6	4.5	8.3	4.3	7.7	4.6	6.6

decrease of d_p value to ca. 4.5 nm. This indicates that the ZIF-8 modification provides a new surface area and an increase in microporosity (pore size < 2 nm), which are both considered beneficial to achieve higher amount of ORR active sites in the catalyst material [50]. According to the literature, the abundant micropores are most likely formed due to the volatilization of Zn during the pyrolysis [17,37]. The S_{BET} value of Fe-N-C is in turn ca. 4 times higher (ca. 600 $m^2\ g^{-1}$) compared to the ZIF-8 modified materials and this value is also well in line with the previous literature reports for various Fe-N-C from Pajarito Powder, LLC [49,51]. This considerably higher S_{BET} value is most likely due to the different types of preparation routes for different catalysts.

XRD measurements were performed to investigate the crystalline phases in the materials and assess the presence of binary TM (alloy) NPs (Fig. 3, Fig. S1). In the case of commercial Fe-N-C, no distinct XRD peaks are observed, while the broad and low intensity graphitic carbon signal could be expected according to the study by Akula et al [49]. In the case of PDC, the distinctive XRD peaks at 26.5°, 43°, and 54.6° are observed corresponding to the graphitic 2H carbon (PDF 01-089-7213), which are in agreement with the previous PDC catalyst investigation [25]. The application of double TM doping during the PDC preparation will introduce a new XRD peak at ca. 45°, which is well observed in the case of CoFe-PDC and CuFe-PDC materials. Very likely this signal corresponds to the presence of monometallic Fe (ICSD 98-018-5742) or binary TM NPs with crystalline structure according to the literature, e.g., FeCo (110) alloy (PDF 65-4131) [52–55]. The modification with ZIF-8 weakens the signals of all XRD peaks indicating the formation of new amorphous material that can partially block the original PDC structure, which could also be explained by the considerable increase in the S_{BET} value (Table 3), while no new distinguishable XRD peaks typical for ZIF-8 or other crystalline ZIF-8 and it`s TM-based structures [56] appeared.

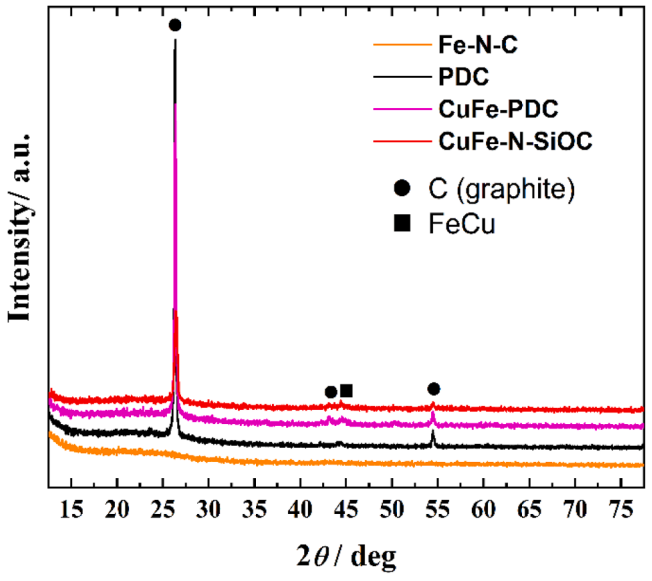

Fig. 3. XRD patterns for Fe-N-C (PMF-014401), transition metal free PDC, Cu and Fe containing catalyst before (CuFe-PDC) and after the ZIF-8 modification (CuFe-N-SiOC).

The XPS analyses were performed to study the surface species and composition of the ZIF-8 modified catalysts (Fig. 4). The survey spectra of the catalysts show the photoelectron peaks of all the elements also observed during the SEM-EDS studies as expected (Table 2). The XP signals of Si2p, Si2s, C1s, and O1s mainly originate from the PDC catalyst support [57–60] and are in good agreement with the previous detailed description by Canuto de Almeida e Silva et al [25].

For the description of ORR performance of TM(s) and N functionalised NPMCs, the high-resolution spectra of corresponding elements should be investigated in more detail. The composition of N1s spectra for Fe-N-C catalysts with various product codes from Pajarito Powder, LLC have been already thoroughly studied in previous reports and as a common observation, the Graphitic-N and Pyridinic-N have been found to be the most prominent components in these N1s spectra [49,61]. Therefore, these two components can be considered very promising for enhancing the performance towards ORR. Especially, it should be considered that the Pyridinic-N can also include the contribution from the transition metal coordinated to nitrogen (M-N_x) sites due to the XPS peak overlapping [56,62], while M-N_x are accepted as the most important N species in this type of catalyst materials promoting $4e^-$ ORR pathway (Eq. 1, Eq. 3) [7,12,33,63,64]. In the case of all three ZIF-8 modified catalysts (Table 4), the N species [46] with the remarkably high relative content of 46-49 % is Pyridinic-N (at ~398.4 eV), which is followed by more variable amounts (11-30 %) of Pyrrolic-N (at ~400.3 eV) and Graphitic-N (at ~401.0 eV). The M-N_x (at ~399.4 eV) and N-oxide (at ~404.2 eV) species are both observed with a relative content between 5-10 %. If the N-oxide component is excluded, then very similar N1s spectra, XPS peak binding energy (BE) values, and component ratios have been recently reported by Kumar et al. for pyrolysed Fe, Co, and ZIF-8 co-doped carbon nanotube-based catalysts [31,32]. In addition to Pyridinic-N, Graphitic-N, and M-N_x, the third major N1s component, Pyrrolic-N, can also play important role for the high ORR activity in acidic and alkaline conditions considering the possible XPS peak overlapping with M-N_x and data from previous reports [49,65,66]. Therefore, all these four N1s components in double TM and ZIF-8 modified materials could be beneficial for the good electrocatalyst performance.

Among TMs, the strong XP signal of Zn introduced by the ZIF-8 modification most likely does not directly contribute to ORR activity under acidic conditions as the centre of the active site (e.g., Zn-N_x), as shown by the study of Martinaiou et al [36]. Remaining TMs (Fe, Co, Mn, Cu) can be considered as the active centres for the M-N_x sites according to the literature [67–69] and therefore are the evidence for the successful preparation of binary TM and N co-doped SiOC catalysts [34, 70–72]. The low signal-to-noise ratio for the collected high-resolution spectra for different TMs, especially for Fe2p and Co2p, could lead to the arbitrary XPS peak deconvolution and content determination, see Fig. S2 [41,45]. Therefore, only the XPS peak maxima for different TM species is presented in Fig. 4e-f to imply the oxidation state of the metal species. For all the ZIF-8 modified catalysts, the lines for Fe^0, Fe^{+2}, and Fe^{+3} at 706.7, 709.6, and 710.8, respectively, show that Fe is most likely in an oxidised form [46,73]. The same conclusion for the TM oxidation state can be made for the Co, Mn, and Cu [46,69]. Whereas, the Mn^{3+} has been reported to enhance O_2 adsorption and electron transfer to O_2, which are beneficial for ORR performance [56,74]. It should be noted that due to the overlapping of Cu^0 and Cu^{1+} XPS peaks these two cannot be distinguished from each other [75]. In the case of CoFe-N-SiOC

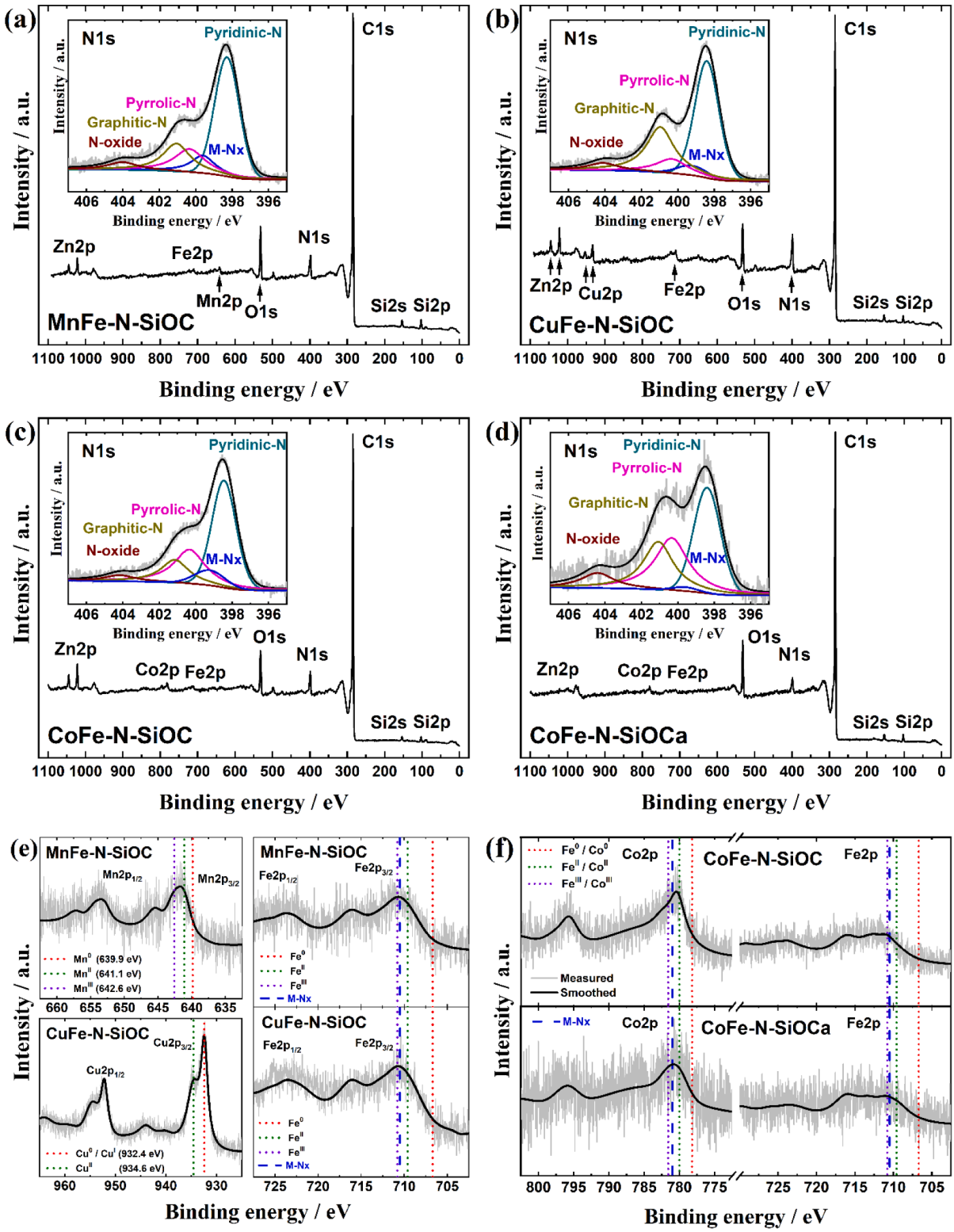

Fig. 4. XPS analysis of different catalyst material powders, (a-d) survey spectra and the inset shows deconvoluted high-resolution XP spectra in N1s region, high-resolution XP spectra in (e, f) Fe2p, (e) Mn2p, Cu2p, and (f) Co2p (Co^0 778.1 eV, Co^{II} 780 eV, Co^{II} 781.6 eV)[46] regions for different catalysts.

catalyst (Fig. 4f), the XPS peak maxima values of $Fe^{+2/+3}$ and $Co^{+2/+3}$ species match very well the experimental binding energy (BE) values reported for the corresponding TM-based M-N_x sites in the literature, ca. 781 eV for Co-N_x and ca. 710.5 eV for Fe-N_x [46,68,76].

The acid leaching of CoFe-N-SiOC catalyst in 2 M H_2SO_4 at 90 °C for 16 h (CoFe-N-SiOCa) resulted in the remarkable decrease in Zn content and an observable increase of O according to the O1s peak height, which is consistent with the oxidising nature of the procedure. According to the N1s peak height, the decreased amount of overall N is observed, which is mainly due to the removal of Pyridinic-N, whereas the Pyridinic-N could be also partially converted to Graphitic-N and N-oxide as their XPS peak contributions have increased.

Table 4
Relative amounts (%) of nitrogen species in different catalyst materials determined from the high resolution N1s XP spectra data shown in the insets to Figs. 4a-d.

Catalyst	Pyridinic-N	M-N_x	Pyrrolic-N	Graphitic-N	N-oxide
MnFe-N-SiOC	49	10	17	19	5
CuFe-N-SiOC	49	5	11	30	5
CoFe-N-SiOC	46	8	26	16	5
CoFe-N-SiOCa	35	2	30	25	8

As the signal to noise ratio in Fe2p region is similar before and after the acid leaching, then one can assume that the Fe content remains rather similar. This could indicate that the surface Fe species are very likely in the form Fe-N_x, which are known to be resistant to acid leaching [77]. According to the analogous observations in Co2p region, the surface Co could be partially removed due to the varying nature of Co species (e.g., co-existence Co nanoparticles, Co-N_x etc.).

HR-TEM images of different ZIF-8 modified catalyst materials (Fig. 5) revealed the PDC structure with TM NPs very similar to the one observed with single TM containing PDCs in an earlier investigation [25]. As a distinct difference, the formation of bamboo-like carbon nanotubes (CNTs) [48,78–80] is observed (Figs. 5a-b) if the double TM doping and ZIF-8 as a N source is used compared to the use of single TM (Co or Ni) and DCDA in our earlier investigation [25]. The formation of CNTs during the high-temperature pyrolysis may be one explanation for the significant increase in the specific surface area during the ZIF-8 modification (Table 3) [29,48,78]. Also, the interconnection of SiOC particles via formed CNTs could be beneficial for enhancing the electron transfer in the catalyst support to the ORR active sites considering that the material contains Si-O rich particles with reduced C content (Fig. 6a). The materials seem to contain both highly amorphous porous C areas (Fig 5d, 20 nm scale bar) with no crystalline signals and parts with typical layered graphitic C lines similar to carbon black (Fig 5b, 10 nm scale bar). There is only some evidence for the preservation of the original ZIF-8 distinct polyhedron structure with ca. 200 nm particle diameter (Fig. 5d) indicating that ultrasonic mixing and pyrolysis have ensured a composite material with uniform distribution and ZIF-8 precursor decomposition or reorganisation. The evidence for reorganisation could be the structural unit with larger size polyhedron formations and uniform binary TM doping (Fig. 5d, Fig. S3b) as previously also observed by Shah et al. for ZIF-8 and double TM-based MnCo-NC/CNT catalyst [56]. The partial loss of pristine ZIF-8 structure is an expected result if

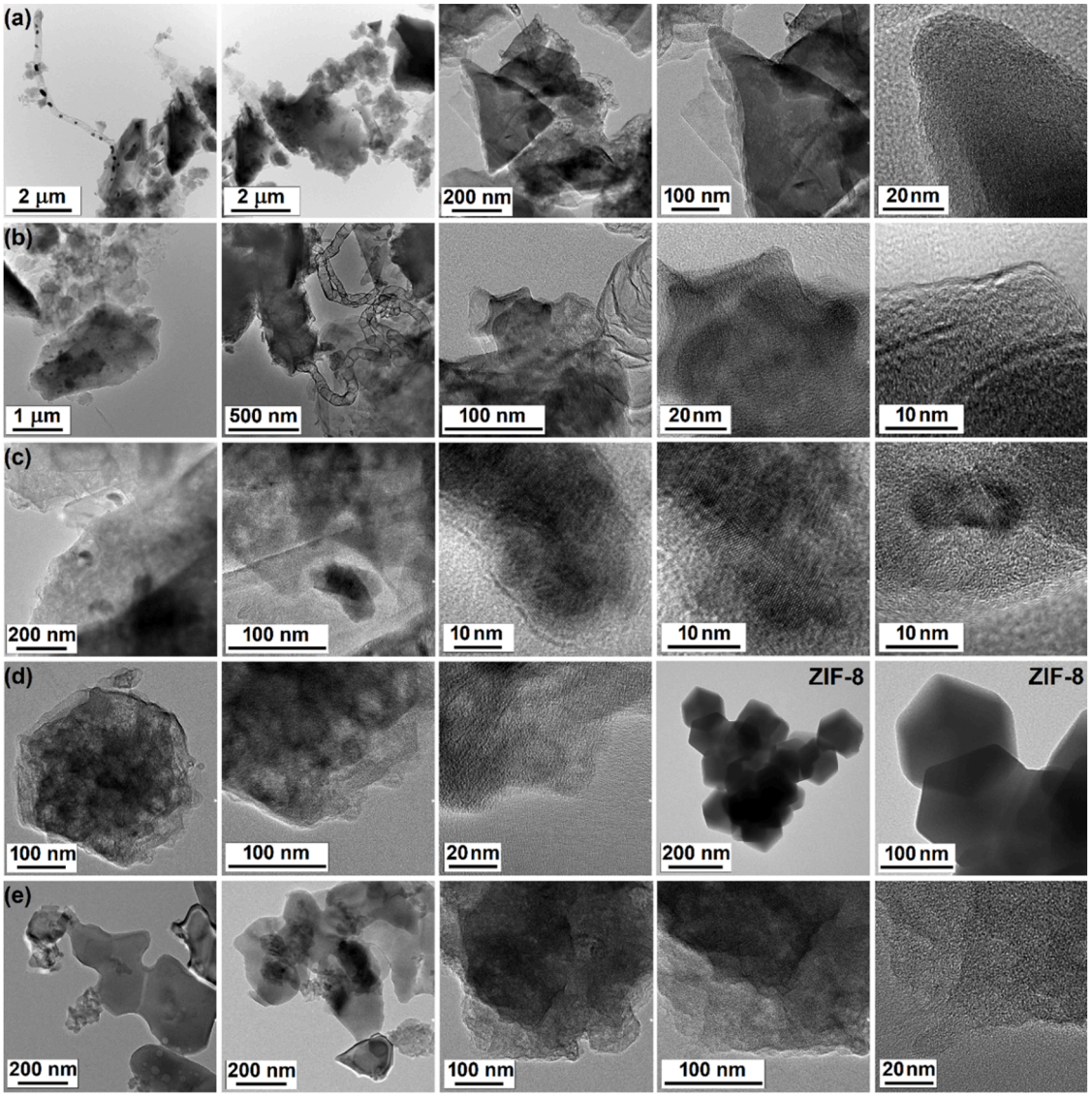

Fig. 5. Bright-field HR-TEM images of (a) CuFe-N-SiOC, (b, c) MnFe-N-SiOC, (d) CoFe-N-SiOC (3 images) and ZIF-8 (Basolite® Z1200, 2 images), (e) CoFe-N-SiOCa catalysts.

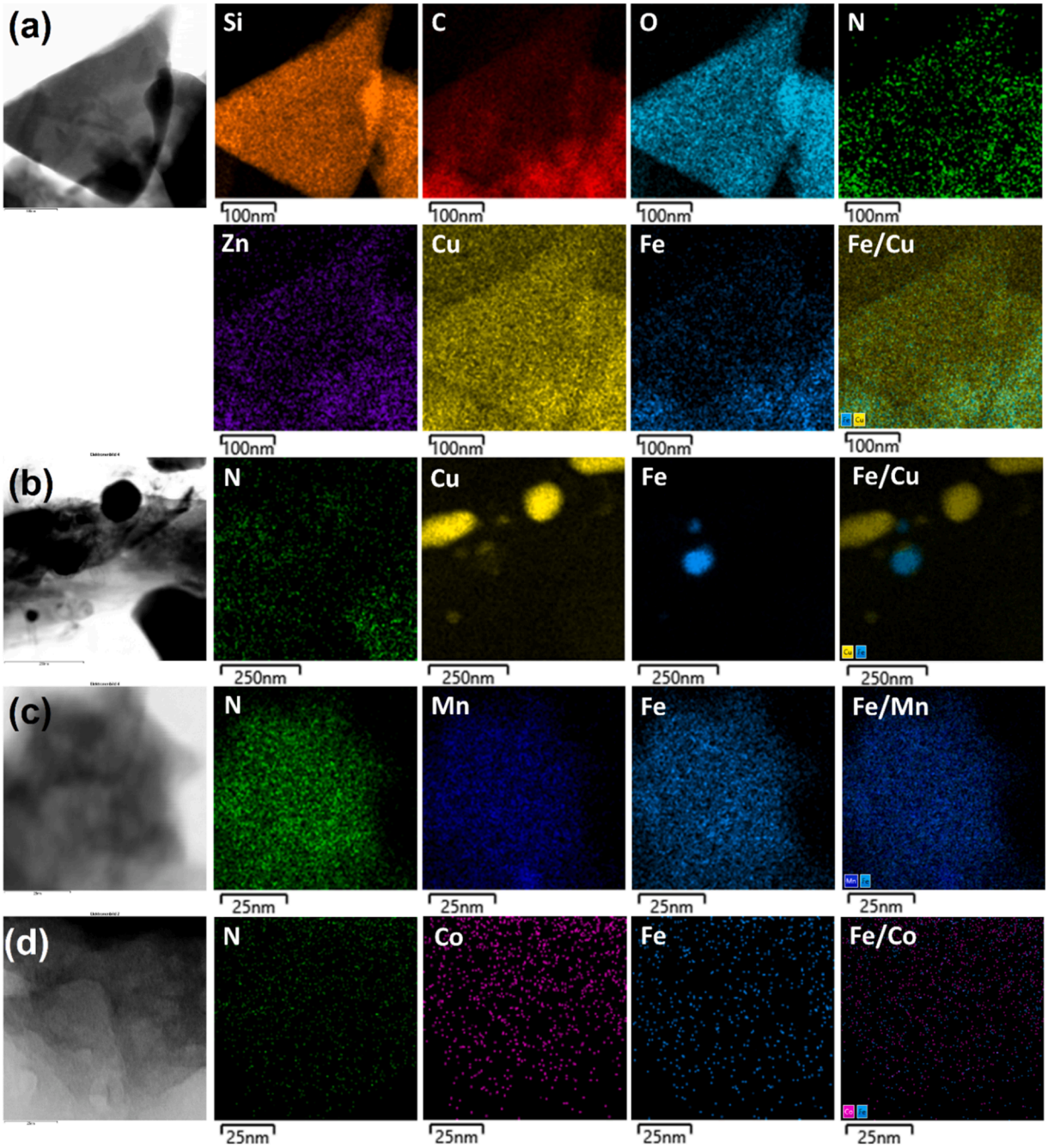

Fig. 6. Bright-field HR-TEM images and corresponding TEM-EDS elemental maps for (a, b) CuFe-N-SiOC, (c) MnFe-N-SiOC, (d) CoFe-N-SiOCa catalysts.

this precursor is considered as a N source to introduce the N-moieties (e.g., Pyridinic-N, M-N_x) into the PDC material (Table 2).

A considerable part of TM NPs (dark spots, Figs. 5a-b, S3a) are observed to be within the CNTs [29], inside the PDC structure or covered with the graphitic carbon layers (Fig. 5c), which can ensure their preservation during the acid leaching and targeted ORR investigations in acidic environment. However, the material must also contain surface or near-surface TM atoms and NPs to explain the formation of nanotubes and XP signals of TMs from the surface characterisation (Fig. 4). The elemental mapping showed the presence of clearly distinguished TM NPs in the case of CuFe-N-SiOC (Fig. 6b), whereas there seems to be presence of monometallic Cu NPs and binary metal FeCu NPs. The latter is in accordance with the FeCu peak appearance in XRD spectra (Fig. 3). All of the studied catalyst materials were found to contain atomically distributed TMs on the tens of nanometres scale indicating to the successful preparation of binary TM and ZIF-8 functionalised NPMCs (Figs. 6c-d, S3b).

3.2. *Half-cell oxygen reduction studies in 0.5 M H_3PO_4 and 0.5 M H_2SO_4*

The preliminary room-temperature ORR half-cell studies in the present work were mainly performed in 0.5 M H_3PO_4 as this environment is more similar to the PA-PBI membrane-based HT-PEMFC devices [1,2]. Firstly, the ORR polarisation curves of commercial Pt/C (20 μg_{Pt} cm^{-2}) and Fe-N-C (0.4 mg cm^{-2}) were recorded at 1600 rpm using the RRDE voltammetry (Fig. 7, Table 5). Good agreement of ORR diffusion-limited current density values (ca. 5.0-5.5 mA cm^{-2}) with previous reports were observed [61,81,82], while the ORR half-wave potential ($E_{1/2}$) was recorded ca. 20-30 mV more positive for both, Pt/C and Fe-N-C, compared to the already published investigations [81,

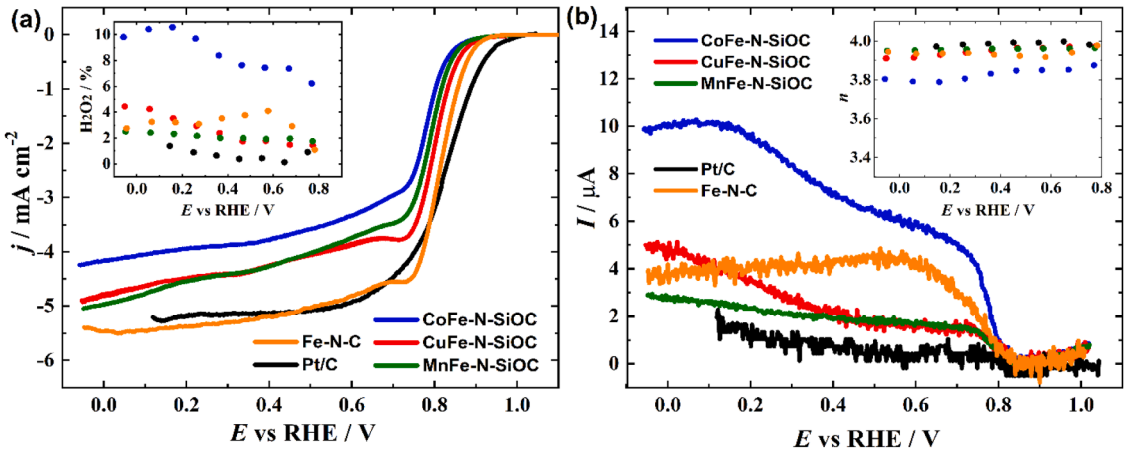

Fig. 7. RRDE voltammetry curves for (a) oxygen reduction at disc, (b) H_2O_2 oxidation at ring on different catalyst coated GC-disc with Pt-ring electrode in O_2-saturated 0.5 M H_3PO_4 at 1600 rpm using 10 mV s^{-1}. The insets to show (a) peroxide yield (%), (b) electron transfer number (*n*) as a function of potential calculated from the RRDE voltammetry curves.

Table 5
ORR half-wave potential ($E_{1/2}$), mass activity values at 0.8 V (MA@0.80V) and 0.85 V (MA@0.85V), average electron transfer number (*n*), average peroxide yield (H_2O_2) obtained from RRDE voltammetry disc and ring curves at 1600 rpm in O_2-saturated 0.5 M H_3PO_4. All the potential values have been obtained from the iR-drop corrected *I-E* curves.

Catalyst	$E_{1/2}$ (mV vs RHE)	MA@0.80V (A g^{-1})	MA@0.85V (A g^{-1})	*n*	H_2O_2 (%)
Pt/C	824 ± 3	74.36 ± 5.84	25.95 ± 2.04	3.99 ± 0.01	0.7 ± 0.4
Fe-N-C	808 ± 2	17.15 ± 0.33	3.82 ± 0.07	3.94 ± 0.02	3.1 ± 0.9
CoFe-N-SiOC	770 ± 3	1.66 ± 0.13	0.27 ± 0.02	3.83 ± 0.03	8.6 ± 1.5
CoFe-N-SiOCa	772 ± 2	1.18 ± 0.11	0.15 ± 0.01	3.70 ± 0.01	14.9 ± 0.2
MnFe-N-SiOC	774 ± 2	2.65 ± 0.11	0.41 ± 0.02	3.96 ± 0.01	2.1 ± 0.3
MnFe-N-SiOCa	757 ± 6	1.64 ± 0.15	0.27 ± 0.02	3.93 ± 0.01	3.6 ± 0.5
CuFe-N-SiOC	781 ± 6	3.55 ± 0.23	0.68 ± 0.04	3.95 ± 0.02	2.7 ± 1.2
CuFe-N-SiOCa	726 ± 8	1.09 ± 0.10	0.22 ± 0.02	3.87 ± 0.01	6.3 ± 0.5

82]. The slightly more positive $E_{1/2}$ values may be influenced by the use of an earlier version of Fe-N-C (NPC-2000, Pajarito Powder, LLC) [81], Pt/C of different origin [81,82], iR-drop correction and differences in catalyst ink preparation (e.g., catalyst to binder ratio, solvent) resulting in a more optimised catalyst layer on the GC electrode. On the other hand, the $E_{1/2}$ value for Fe-N-C reported herein is very similar to the one observed for non-commercial BP-FeNC prepared in the work by Hu et al. with 0.6 mg cm^{-2} catalyst loading [81]. The H_2O_2 yield and electron transfer number (*n*) were calculated from the ring and disc current according to the equations from earlier report [65]. In the case of Pt/C, a very low average H_2O_2 yield and mean *n* values of 0.7 % and 3.99 are observed indicating the expected 4e⁻ ORR pathway (Eq. 1). The average *n* value for Fe-N-C is slightly lower at 3.94, together with the higher H_2O_2 yield (3.1 %), indicating that latter amount of O_2 molecules is reduced via the 2e⁻ route (Eq. 2).

The ORR performance of unmodified double TM containing PDC materials (catalyst loading 0.8 mg cm^{-2}) was rather poor according to the low oxygen reduction current density and high H_2O_2 yield (Fig. S4). The functionalisation of binary TM containing PDCs with N was firstly performed using DCDA as a N source similarly to the procedure from our earlier investigations with single TM containing PDCs [25] and double TM (Fe, Co) co-doped graphene-coated alumina nanofibers [46]. The N-functionalisation with DCDA is beneficial for the reduction of peroxide yield (e.g., MnFe-PDC-N), while the oxygen reduction performance is still considerably lower compared to the one of Fe-N-C (Fig. S5). Furthermore, optimisation of the pyrolysis temperature and PDC:DCDA weight ratio in the precursor mixture has no significant effect on the ORR performance in 0.5 M H_3PO_4 (Fig. S5c).

As an alternative functionalisation procedure, the use of ZIF-8 as a N source was adapted from more recent investigations, in which binary TM (Fe, Co) and N co-doped CNT-based catalyst materials were prepared [31,32]. As the MnFe-PDC exhibited the highest ORR performance after N-functionalisation with DCDA, then MnFe-PDC was chosen for optimisation of N-doping procedure with ZIF-8. In brief, three different pyrolysis temperatures (900, 950, and 1000 °C) together with several PDC:ZIF-8 weight ratios were applied to MnFe-PDC material (Fig. S6a). The highest activity towards the ORR was obtained at a ratio of 1:1 and 950 °C, which was also used for two other double TM material modifications (Fig. 7, Table 5). The ZIF-8 modification leads to catalyst materials that exhibit significantly higher ORR activity compared to the DCDA route and closely approximate to Fe-N-C performance. The higher general ORR activity obtained with ZIF-8 compared to the DCDA could be due to the Zn atoms being able to effectively restrain aggregation of other (ORR active) TMs into NPs during pyrolysis, resulting in a higher relative amount of TM-N_x sites (e.g., Cu-N_x, Fe-N_x etc.) [17,37,38,73].

The lowest diffusion limiting current and highest peroxide yield (average 8.6 %, Fig 7a) among ZIF-8 modified binary TM catalysts is obtained in the case of CoFe-N-SiOC, which can be expected as Co-N_x sites have been reported to promote the 2e⁻ ORR pathway (Eq. 2) [68]. The average peroxide yields for CuFe-N-SiOC (2.7 %) and MnFe-N-SiOC (2.1 %) in Fig. 7a (Table 5) are lower than the one of Fe-N-C indicating that both additional metals could contribute to the 4e⁻ ORR pathway (Eq. 1, Eq. 3) by reduction of formed H_2O_2 or lowering the reaction energy barrier of Fe-N_x sites [71]. The CuFe-N-SiOC catalyst shows the most positive $E_{1/2}$ value of ca. 0.78 V among the catalysts prepared in the present work, which is in accordance with the literature as double Cu-N_x and Fe-N_x site containing nanocarbon materials have been reported to be highly active for ORR in acidic and alkaline conditions according to experimental and computational studies [70,71,83]. In the H_3PO_4 solution, the high ORR performance of Fe and Cu co-doped NPMCs can be attributed to the synergistic role of the neighbouring Cu and Fe atoms with an appropriate distance according to the study by Cheng et al [83]. To our knowledge, this is the very first study describing the ORR performance of binary TM-based NPMCs specifically in the 0.5 H_3PO_4 solution, while various highly active Fe-N-C type of ORR catalyst with the $E_{1/2}$ value between ca. 0.73-0.81 V have been previously reported [61,81].

Additionally, the CV response of ZIF-8 modified double TM catalysts was compared to the one of Fe-N-C using a potential scan rate of 50 mV s^{-1} in Ar- and O_2-saturated 0.5 M H_3PO_4 (Fig. S7). Surprisingly, all catalyst materials exhibited a very similar ORR peak potential (E_p) value of ca. 0.655 V vs RHE under stationary conditions indicating the superiority of investigations under hydrodynamic conditions (e.g., RRDE). To evaluate the stability of the catalysts, an accelerated durability test (ADT) protocol was carried out, comprising 10 000 CV cycles (100 mV s^{-1}) between 1.0 and 0.6 V vs RHE and a RRDE measurement at 1600 rpm before and after the cycling (Fig. S8). There is no prior known RRDE half-cell stability testing data for Fe-N-C in H_3PO_4 solution, while the negative half-wave potential shift ($\Delta E_{1/2}$) of 30-40 mV has already been reported in 0.5 M H_2SO_4 after using a very similar ADT protocol [49]. Since a $\Delta E_{1/2}$ value of only 18 mV was observed here for Fe-N-C, it can be concluded that H_3PO_4 solution could be less degrading for the NPMC materials compared to H_2SO_4 medium. Among ZIF-8 modified binary TM catalysts, only CoFe-N-SiOC showed promising durability similar to Fe-N-C, while CuFe-N-SiOC and MnFe-N-SiOC exhibited poorer $\Delta E_{1/2}$ values of more than 30 mV.

Since the acid treatment procedure can considerably increase the ORR activity of the double TM-doped NPMCs [41,55] and help to evaluate the suitability of the material for harsh HT-PEMFC conditions (saturated H_3PO_4 at 160 °C) [1], two comparable acid leaching routes from previous investigations were applied [39–41]. Surprisingly, the 3 M H_2SO_4 + HNO_3 route was found to be significantly detrimental for the ORR activity of the MnFe-N-SiOC catalyst, while the 2 M H_2SO_4 treatment did not have such a significant effect on the ORR performance (Fig. S6b) and also exhibited ca. 15 % higher material recovery yield. The more promising 2 M H_2SO_4 route was also applied for the other two catalysts, CoFe-N-SiOC and CuFe-N-SiOC (Fig. 8, Table 5). As a common observation, the acid treatment has a similar negative effect on the mass activity values, higher peroxide yield and a corresponding decrease in the diffusion limiting current for all three materials.

The CoFe-N-SiOCa catalyst showed the lowest n value (3.70, Table 5), which was also calculated in parallel using the Koutecky-Levich (K-L) equation and parameter values from the investigation by Kumar et al [82]. The calculations using the slopes of the K-L lines of j-E curves recorded at different rotation rates resulted in a very similar average n value of approximately 3.63 (Fig. S9). It should be mentioned that MnFe-N-SiOCa peroxide yield remains the lowest (average 3.6 %, Table 5) and is still comparable to the one of Fe-N-C. Furthermore, the Cu/Fe materials show a considerable decrease of ca. 50 mV in the $E_{1/2}$ value, which indicates that this binary TM combination in NPMC is less likely suitable for the use in high-temperature acidic environment. This decrease could be due to the loss of TM-N_x sites that were present on the TM (alloy) NPs (Fig. 6b) and were removed during acid leaching. On the other hand, the $E_{1/2}$ value of Co/Fe catalyst remains basically unchanged and furthermore, a peculiar wave-like increase in the O_2 reduction current at ca. 0.7 V has appeared. This wave-like increase is known to appear in the case of Fe and/or Co co-doped NPMCs also in 0.5 M H_2SO_4 [84–86] and its intensity is known to decrease with higher rotation rates as also observed here for CoFe-N-SiOCa (Fig. S9a) [55]. Since the oxygen reduction curve of Fe-N-C at approx. 0.75 V has a similar shape, this catalyst was investigated together with CoFe-N-SiOCa with different catalyst loadings (Fig. 9a). A clear dependence between the intensity of wave-like increase and catalyst loading was observed, indicating that the phenomenon is most likely due to the O_2 trapped/pre-adsorbed in the thick and highly porous NPMC layer, as both the increase in rotation rate and decrease in catalyst loading both help to suppress this wave due to the enhanced mass transfer in the catalyst layer (CL).

A similar dependence on catalyst loading was previously also observed by Wu et al. for Fe/Co-CNT in 1 M KOH [87]. The occurrence of this wave for CoFe-N-SiOCa could indicate the higher number of accessible TM-N_x sites exposed during acid leaching due to the removal of blocking and inactive Zn species according to the XPS studies (Fig. 4). The CoFe-N-SiOCa catalyst was also subjected to ADT with 10 000 CV cycles and a considerably higher ORR stability ($\Delta E_{1/2}$ = 8 mV, Fig. 9b) was observed compared to the Fe-N-C and non-acid treated catalyst version (Fig. S8). At the same time, the durability of CuFe-N-SiOCa and MnFe-N-SiOCa has decreased after the acid treatment (Fig. S10) indicating that CoFe-N-SiOCa could be the most suitable material for the harsh HT-PEMFC conditions [1].

To additionally evaluate the activity and stability of CoFe-N-SiOC(a) catalysts towards ORR, the comparison RRDE measurements were also carried out in more commonly used 0.5 M H_2SO_4 environment (Fig. S11, Table S1). All three studied catalysts show the $E_{1/2}$ value ca. 80-100 mV more negative compared to the results obtained in 0.5 M H_3PO_4 (Tables 5 and S1). Furthermore, the $E_{1/2}$ values decreased more by ca. 30-50 mV if two times lower catalyst loading was used for comparison in 0.5 M H_2SO_4. Nevertheless, the $E_{1/2}$ value of 0.71 V for Fe-N-C (0.2 mg cm^{-2}) is in good agreement with the previously reported ones for different Fe-N-C from Pajarito Powder, LLC [49]. ADT test in 0.5 M H_2SO_4 environment (Fig. S12) revealed that the superiority of CoFe-N-SiOCa catalyst in ORR durability compared to the Fe-N-C as observed in the case of 0.5 M H_3PO_4 solution (Figs. S8, 9b) was not witnessed most likely due to the harsher conditions (pH = 0.3 vs 1.26). This observation can indicate that 0.5 M H_3PO_4 could be more suitable environment for the initial screening of catalyst materials for PA-PBI membrane-based HT-PEMFC application.

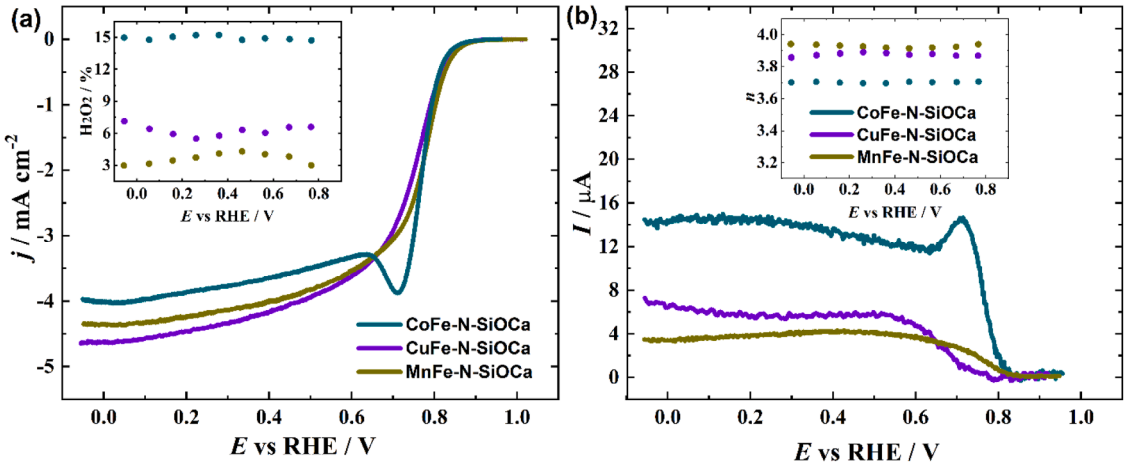

Fig. 8. RRDE voltammetry curves for (a) oxygen reduction at disc, (b) H_2O_2 oxidation at ring on different catalyst coated GC-disc with Pt-ring electrode in O_2-saturated 0.5 M H_3PO_4 at 1600 rpm using 10 mV s^{-1}. The insets to show (a) peroxide yield (%), (b) electron transfer number (n) as a function of potential calculated from the RRDE voltammetry curves.

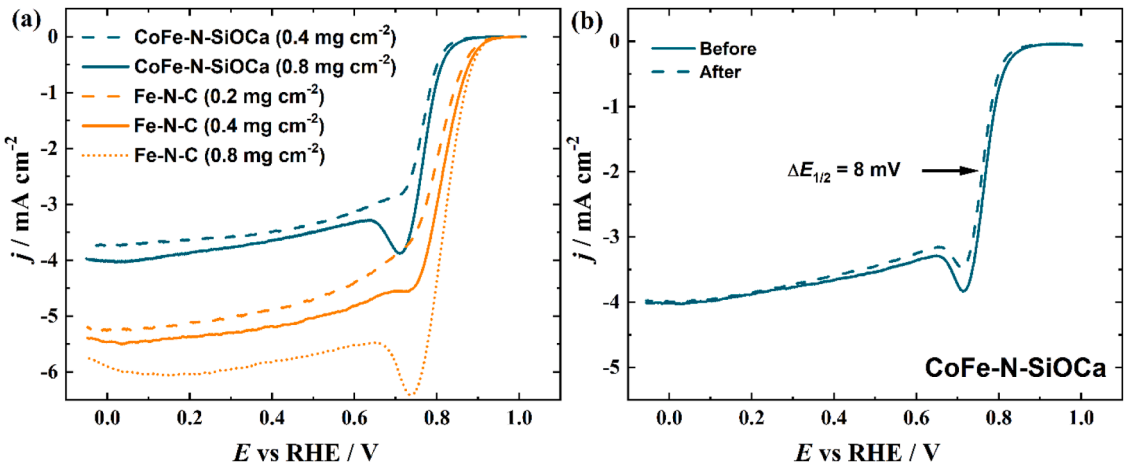

Fig. 9. RRDE voltammetry curves for oxygen reduction at disc recorded with (a) CoFe-N-SiOCa, Fe-N-C catalysts with different loading, (b) before (solid line) and after (dashed line) 10 000 CV cycles with CoFe-N-SiOCa (0.8 mg cm^{-2}) in O_2-saturated 0.5 M H_3PO_4 at 1600 rpm (v = 10 mV s^{-1}).

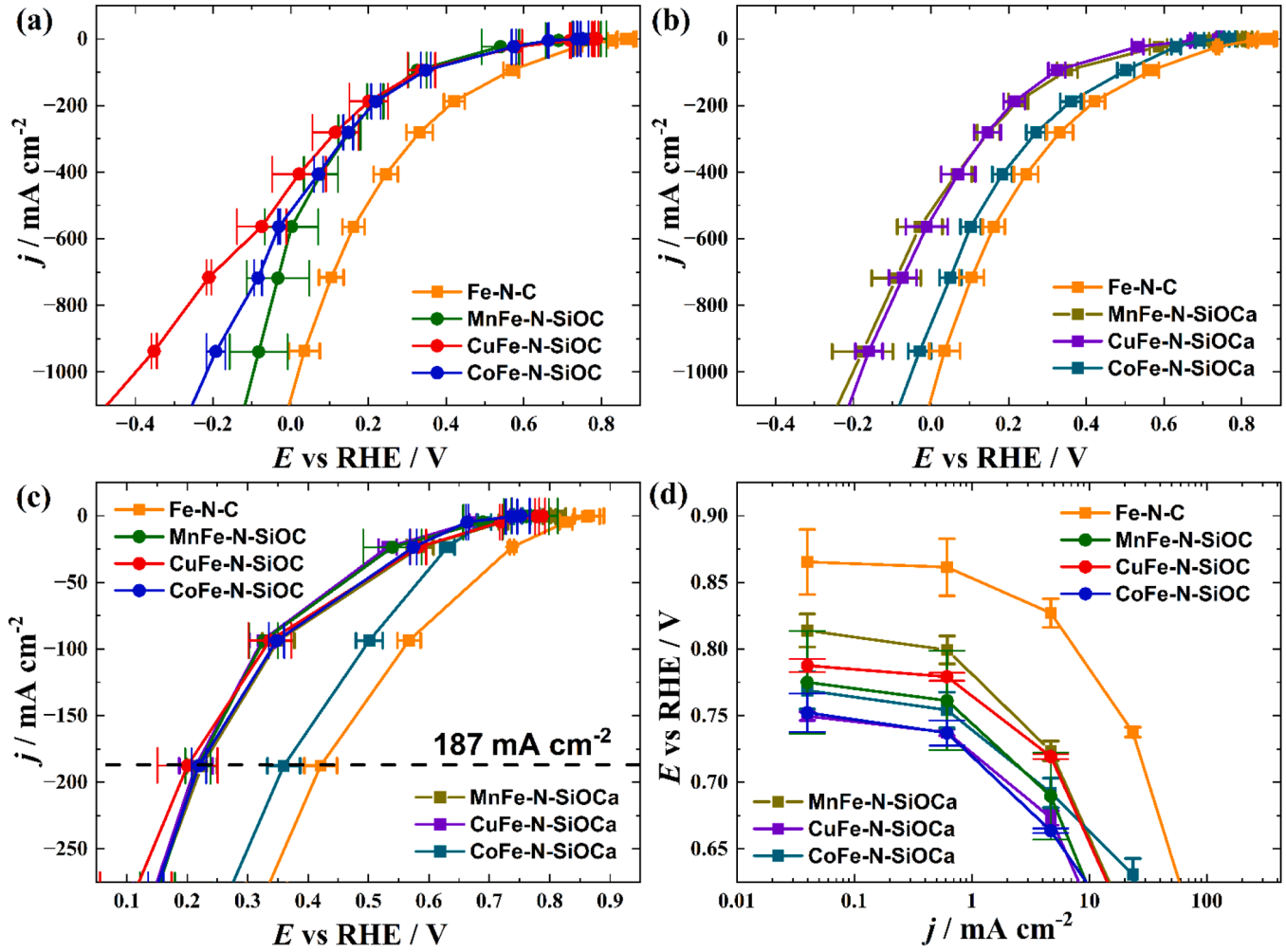

Fig. 10. (a) Polarisation curves of (a, c) ZIF-8-modified and (b, c) further acid leached catalyst based GDEs, (d) semi-logarithmic plots of the activation areas of the polarisation curves from Fig. c. The measurement was performed in a GDE half-cell setup (O_2 flow rate 0.15 L min^{-1}, 160 °C, conc. H_3PO_4).

3.3. GDE half-cell and HT-PEMFC testing

To further evaluate the ORR performance of the catalysts under HT-PEMFC conditions, the GDE half-cell setup with an operating temperature of 160 °C and conc. H_3PO_4 electrolyte was used. The same catalyst ink composition optimised for the Fe-N-C catalyst (40 wt% PTFE) in our previous investigation was used for all double TM and N co-coped NPMCs prepared in this work [44]. As a difference, a simple drop casting method instead of ultrasonic spray coating was used in the present investigation for CL preparation. Firstly, the Fe-N-C polarisation

Table 6
Half-cell GDE testing results, open circuit potential (OCP) and potential value at 187 mA cm^{-2} (E_{187}) for ORR derived from the GDE polarisation curves with different cathode catalyst materials shown in Fig. 10.

Catalyst	OCP (mV vs RHE)	E_{187} (mV vs RHE)
Fe-N-C	865 ± 24	421 ± 27
CoFe-N-SiOC	752 ± 15	219 ± 12
CoFe-N-SiOCa	769 ± 14	360 ± 27
MnFe-N-SiOC	775 ± 38	218 ± 21
MnFe- N-SiOCa	814 ± 12	224 ± 25
CuFe-N-SiOC	788 ± 15	201 ± 50
CuFe- N-SiOCa	750 ± 13	214 ± 28

curve obtained here is more similar to the curve with lower ORR activity at 10 wt% PTFE from a previous investigation [44] throughout the studied current density (*j*) values, which is most likely due to the different CL fabrication method (Fig. 10, Table 6). Also, the CVs recorded with N_2-flow at the GDE before and after the GDE testing are in good agreement with the previous results (Fig. S13a) [44]. The ZIF-8 modified materials (-N-SiOC) all show similar lower ORR activity compared to the Fe-N-C (Fig. 10a) and performance differences are observed at higher *j* values (>600 mA cm^{-2}), with MnFe-N-SiOC being the most active and CuFe-N-SiOC the least active catalyst. The acid treatment procedure decreases the ORR performance differences between the CuFe and MnFe materials, while CoFe-N-SiOCa has become much more active and approaches Fe-N-C (Fig. 10b). The situation is to some extent similar to the 0.5 M H_3PO_4 half-cell test (appearance of a peculiar wave-like increase, Fig. 8a), while no such advantage for CoFe-N-SiOCa was observed in 0.5 M H_2SO_4 (Fig. S11). The CVs recorded before and after the ORR study with an N_2 flow at the GDE show no influence of the acid treatment on the catalyst behaviour (Fig. S13b and c). From the point of view of HT-PEMFC applications, only the potentials higher than approx. 0.2 V vs RHE are of interest, where the superiority of CoFe-N-SiOCa can be clearly seen (Fig. 10c, Table 6).

The semi-logarithmic plot of the low current density region enables the observation of activation polarisation area close to the open circuit potential (OCP) value (Fig. 10d, Table 6). The acid leaching seems to be beneficial for the Co/Fe and Mn/Fe materials to achieve higher OCP, while Cu/Fe shows a significant decrease in OCP similarly to 0.5 M H_3PO_4 (Table 5). The poor performance of Cu/Fe materials is a somewhat controversial result because while Cu^{2+} has recently been reported to be poisonous/detrimental for the LT-PEMFC components [88], one of the most remarkable NPMC cathode catalyst results for HT-PEMFC was obtained with a Pt-free atomically dispersed bimetallic FeCu catalyst in the study by Cheng et al [83]. Cu nanoparticles observed in this work for CuFe-N-SiOC (Fig. 6b) could be the source for free Cu^{2+} ions released into the PA-PBI membrane causing a decrease in catalyst activity and/or membrane ionic conductivity. While MnFe-N-SiOCa catalyst shows the highest performance in the activation polarisation region (>0.675 V vs RHE), CoFe-N-SiOCa remains as the most promising catalyst for achieving high current density values and high durability (Fig. 9b).

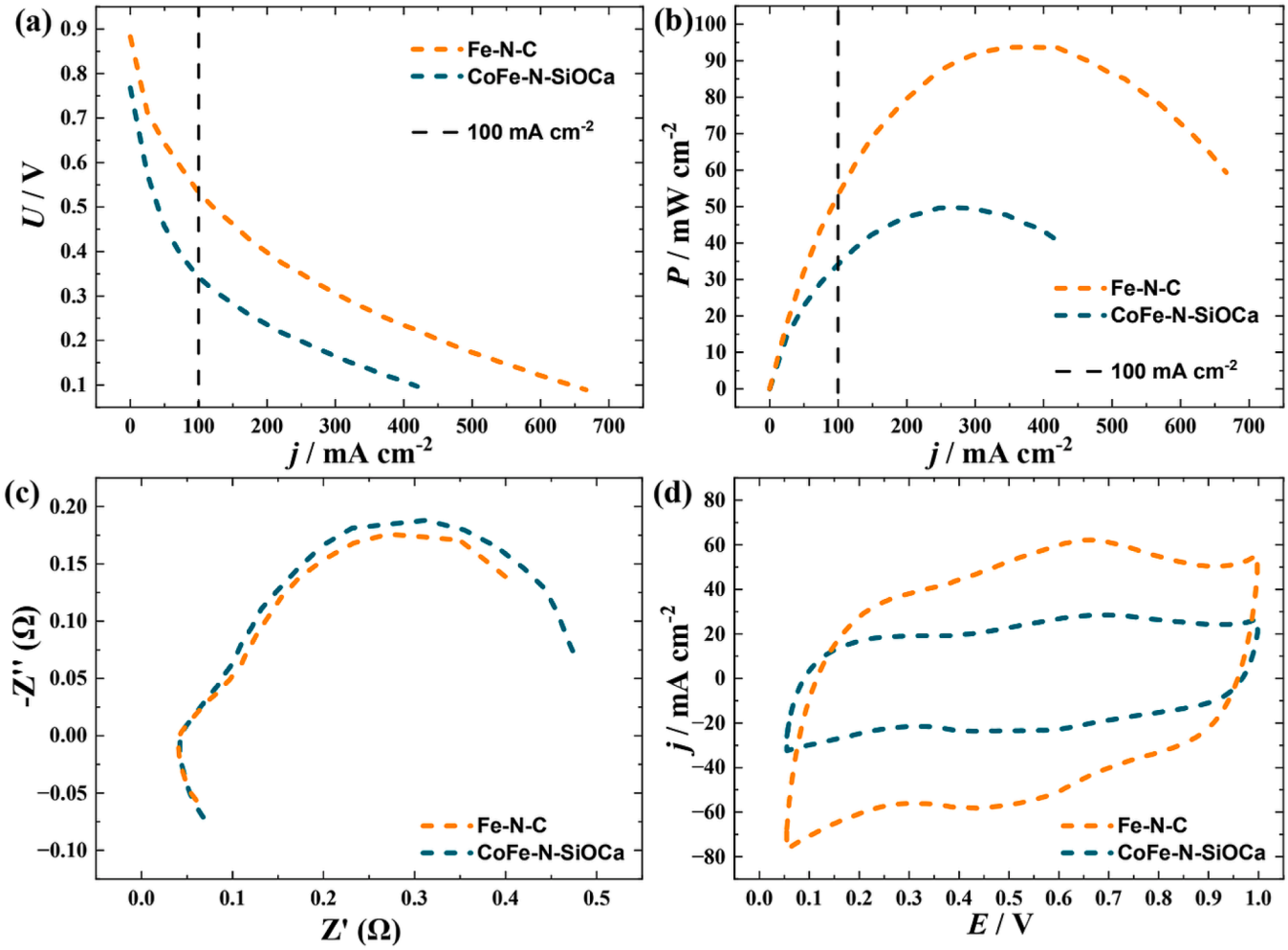

Fig. 11. HT-PEMFC measurement data with CoFe-N-SiOCa and Fe-N-C (PMF-014401) cathode catalysts (3 mg cm^{-2}), (a) galvanostatic polarization curves recorded under H_2/O_2 (1.5/9.5) at 160 °C, (b) calculated power density curves, (c) Nyquist plots from EIS at 0.1 A cm^{-2} recorded with dry H_2/O_2 (1.5/9.5), (d) CVs of cathode recorded with scan rate of 100 mV s^{-1} under N_2 flow rate of 0.1 L min^{-1}.

Considering the previous observations, CoFe-N-SiOCa was chosen to be tested as cathode in HT-PEM single cell and compared to an Fe-N-C-based MEA (Fig. 11). Different from previous investigations [10,61], the CL at the cathode was prepared via drop-casting in the present work. Very similar HT-PEMFC performance was registered for Fe-N-C (open circuit voltage (OCV) = 883 mV, power density at 100 mA cm^{-2} (P_{100}) = 53 mW cm^{-2}) compared to the corresponding values reported earlier for HT-PEMFC with ultrasonic spray coated and doctor blade coated Fe-N-C (PMF-011904, Pajarito Powder) cathodes [61]. The OCV and P_{100} values for CoFe-N-SiOCa are lower with values of 768 mV and 34 mW cm^{-2}, respectively. The performance difference between CoFe-N-SiOCa and Fe-N-C is most likely due to the ORR activity of the cathode catalysts as the ohmic resistance of both MEAs is very similar (Fig. 11c). For comparison, in the case of atomically dispersed bimetallic FeCu catalyst in the study by Cheng et al [83], the higher P_{100} = ~70 mW cm^{-2} (FeCu (4:1) 160 °C) can be found with a NPMC loading of 4 mg cm^{-2}. For the present study, it can be concluded that the performance trend of GDE half-cell measurements and HT-PEMFC tests are same.

The CV curves recorded from the cathode revealed the reversible redox peaks at ca 0.6 V (Fig. 11d), which have been also observed previously for Fe-containing NPMC cathodes in HT-PEMFC and could correspond to redox couples of hydroquinone/quinone and Fe^{2+}/Fe^{3+} [10,61]. The higher capacitive current under the CV curve in the case of Fe-N-C compared to Co-Fe-N-SiOCa can refer to the considerably higher SSA of Fe-N-C (Table 3). For the future perspective, the further optimization of SSA and electrode fabrication could boost the overall HT-PEMFC performance as the used cathode ink recipe has been optimized for Fe-N-C [44].

Mainly based on the ADT results recorded in 0.5 M H_3PO_4 (Figs. S8, 9b), the observed higher stability of Co and Fe co-doped NPMC due to the Co atoms has been previously well documented [20,89] together with the higher ORR activity provided by the inclusion of Co [54,87] and possible suppression of Fenton reactions [20,90]. Therefore, the CoFe-N-SiOCa catalyst preparation route among the experimental NPMC presented herein may be the most promising one to advance the preparation of polymer-derived ceramic electrocatalysts for HT-PEMFC cathodes with two transition metals and ZIF-8 functionalization.

4. Conclusions

In the present investigation, the binary transition metal and N functionalised NPMC materials were prepared via pyrolysis using PDCs with three different TM combinations, Fe/Cu, Fe/Mn, Fe/Co. Two N sources were compared (DCDA and ZIF-8) and the ZIF-8 route was found to be superior for HT-PEMFC cathode catalyst application. All ZIF-8 modified catalyst materials exhibited S_{BET} of ca. 130-140 m^2 g^{-1}, hierarchical porosity, and the presence of TM (alloy) NPs together with atomically dispersed TMs. The ORR activity studies revealed that Fe/Co containing and acid leached catalyst material (CoFe-N-SiOCa) exhibited the highest long-term durability in 0.5 M H_3PO_4 solution ($\Delta E_{1/2}$ of only 8 mV) and the highest overall ORR activity during high-temperature GDE testing in conc. H_3PO_4. The MnFe-N-SiOCa catalyst showed the lowest hydrogen peroxide yield (3.6 %) in 0.5 M H_3PO_4 medium and the highest OCP (814 mV vs RHE) in the harsher GDE testing conditions. HT-PEMFC testing with drop-cast CoFe-N-SiOCa cathode showed P_{100} = 34 mW cm^{-2} and OCV = 768 mV, while similarly prepared Fe-N-C cathode exhibited P_{100} = 53 mW cm^{-2} and OCV = 883 mV.

CRediT authorship contribution statement

Marek Mooste: Writing – review & editing, Writing – original draft, Resources, Project administration, Methodology, Investigation, Funding acquisition, Formal analysis, Data curation, Conceptualization. **Julia Müller-Hülstede:** Data curation, Formal analysis, Investigation, Methodology, Software, Supervision, Validation, Writing – review & editing. **Dana Schonvogel:** Writing – review & editing, Writing – original draft, Supervision, Methodology, Funding acquisition, Formal analysis, Data curation. **Tanja Zierdt:** Writing – review & editing, Writing – original draft, Methodology, Formal analysis, Data curation. **Julia Buschermöhle:** Data curation, Formal analysis, Investigation, Methodology, Software, Supervision, Validation, Writing – review & editing. **Killian Fuhrmann:** Writing – review & editing, Writing – original draft, Methodology, Investigation, Data curation. **Michaela Wilhelm:** Writing – review & editing, Writing – original draft, Supervision, Methodology, Investigation, Formal analysis, Data curation, Conceptualization. **Peter Wagner:** Writing – review & editing, Writing – original draft, Supervision, Resources, Project administration, Methodology, Funding acquisition, Conceptualization. **K. Andreas Friedrich:** Writing – review & editing, Writing – original draft, Supervision, Project administration, Methodology, Funding acquisition, Conceptualization.

Declaration of competing interest

The authors declare that they have no known competing financial interests or personal relationships that could have appeared to influence the work reported in this paper.

Acknowledgements

This study was financially supported by the Estonian Research Council grant (PUTJD1170). M. M. acknowledges DLR and the German Academic Exchange Service (DAAD) for the funding via DLR-DAAD Research Fellowship No. 521. The XPS instrument is funded by German Research Foundation (DFG) through grants INST 184/144-1 FUGG. The authors acknowledge the Electron and Light Microscopy Service Unit, Carl von Ossietzky University of Oldenburg, for the use of the imaging facilities. We would like to thank Stefanie Laue (DLR) for performing HT-PEMFC measurements.

Supplementary materials

Supplementary material associated with this article can be found, in the online version, at doi:10.1016/j.electacta.2024.145620.

Data availability

Data will be made available on request.

References

[1] Q. Meyer, C.J. Yang, Y. Cheng, C. Zhao, Overcoming the electrode challenges of high-temperature proton exchange membrane fuel cells, Electrochem. Energy Rev. 6 (2023) 16.
[2] A. Zucconi, J. Hack, R. Stocker, T.A.M. Suter, A.J.E. Rettie, D.J.L. Brett, Challenges and opportunities for characterisation of high-temperature polymer electrolyte membrane fuel cells: a review, J. Mater. Chem. A 12 (2024) 8014–8064.
[3] S.S. Araya, F. Zhou, V. Liso, S.L. Sahlin, J.R. Vang, S. Thomas, X. Gao, C. Jeppesen, S.K. Kaer, A comprehensive review of PBI-based high temperature PEM fuel cells, Int. J. Hydrog. Energy 41 (2016) 21310–21344.
[4] J.L. Zhang, Z. Xie, J.J. Zhang, Y.H. Tanga, C.J. Song, T. Navessin, Z.Q. Shi, D. T. Song, H.J. Wang, D.P. Wilkinson, Z.S. Liu, S. Holdcroft, High temperature PEM fuel cells, J. Power Sources 160 (2006) 872–891.
[5] K. Mishra, N. Devi, S.S. Siwal, V.K. Thakur, Insight perspective on the synthesis and morphological role of the noble and non-noble metal-based electrocatalyst in fuel cell application, Appl. Catal. B-Environ. 334 (2023) 122820.
[6] S. Zago, L.C. Scarpetta-Pizo, J.H. Zagal, S. Specchia, PGM-free biomass-derived electrocatalysts for oxygen reduction in energy conversion devices: promising materials, Electrochem. Energy Rev. 7 (2024) 1.
[7] A. Sarapuu, J. Lilloja, S. Akula, J.H. Zagal, S. Specchia, K. Tammeveski, Recent advances in non-precious metal single-atom electrocatalysts for oxygen reduction reaction in low-temperature polymer-electrolyte fuel cells, ChemCatChem 15 (2023) e202300849.
[8] N. Seselj, D. Aili, S. Celenk, L.N. Cleemann, H.A. Hjuler, J.O. Jensen, K. Azizi, Q. F. Li, Performance degradation and mitigation of high temperature polybenzimidazole-based polymer electrolyte membrane fuel cells, Chem. Soc. Rev. 52 (2023) 4046–4070.

[9] F. Jaouen, D. Jones, N. Coutard, V. Artero, P. Strasser, A. Kucernak, Toward platinum group metal-free catalysts for hydrogen/airproton-exchange membrane fuel cells, Johns. Matthey Technol. Rev. 62 (2018) 231–255.

[10] J. Müller-Hülstede, H. Schmies, D. Schonvogel, Q. Meyer, Y. Nie, C. Zhao, P. Wagner, M. Wark, What determines the stability of Fe-N-C catalysts in HT-PEMFCs? Int. J. Hydrog. Energy 50 (2024) 921–930.

[11] N. Seselj, S.M. Alfaro, E. Bompolaki, L.N. Cleemann, T. Torres, K. Azizi, Catalyst development for high-temperature polymer electrolyte membrane fuel cell (HT-PEMFC) applications, Adv. Mater. 35 (2023) 2302207.

[12] M.A. de Araujo, A.A. Koverga, A.M.P. Sakita, F.B. Ometto, L.G. da Trindade, E. A. Ticianelli, M-N-C materials for electrochemical reduction reactions: recent strategies for improving electrocatalytic activity and stability, ChemCatChem 15 (2023) e202201594.

[13] H.B. Tan, J. Tang, J. Kim, Y.V. Kaneti, Y.M. Kang, Y. Sugahara, Y. Yamauchi, Rational design and construction of nanoporous iron- and nitrogen-doped carbon electrocatalysts for oxygen reduction reaction, J. Mater. Chem. A 7 (2019) 1380–1393.

[14] A. Pedersen, J. Barrio, A.L. Li, R. Jervis, D.J.L. Brett, M.M. Titirici, I.E.L. Stephens, Dual-metal atom electrocatalysts: theory, synthesis, characterization, and applications, Adv. Energy Mater. 12 (2022) 2102715.

[15] F. Luo, A. Roy, M.T. Sougrati, A. Khan, D.A. Cullen, X.L. Wang, M. Primbs, A. Zitolo, F. Jaouen, P. Strasser, Structural and reactivity effects of secondary metal doping into iron-nitrogen-carbon catalysts for oxygen electroreduction, J. Am. Chem. Soc. 145 (2023) 14737–14747.

[16] M. Alam, K. Ping, M. Danilson, V. Mikli, M. Käärik, J. Leis, J. Aruväli, P. Paiste, M. Rähn, V. Sammelselg, K. Tammeveski, S. Haller, U.I. Kramm, P. Starkov, N. Kongi, Iron triad-based bimetallic M–N–C nanomaterials as highly active bifunctional oxygen electrocatalysts, ACS Appl. Energy Mater. 7 (2024) 4076–4087.

[17] Y. Meng, J.X. An, P.X. Hou, C. Liu, J.C. Li, Atomically dispersed Fe/Co-N-C and their composites for proton exchange membrane fuel cells, Mater. Chem. Front. 8 (2024) 1927–1949.

[18] B. Jaleh, M. Nasrollahzadeh, M. Eslamipanah, A. Nasri, E. Shabanlou, N. R. Manwar, R. Zboril, P. Fornasiero, M.B. Gawande, The role of carbon-based materials for fuel cells performance, Carbon 198 (2022) 301–352.

[19] S.Y. Liu, Q. Meyer, C. Jia, S.H. Wang, C.L. Rong, Y. Nie, C. Zhao, Operando deconvolution of the degradation mechanisms of iron-nitrogen-carbon catalysts in proton exchange membrane fuel cells, Energy Environ. Sci. 16 (2023) 3792–3802.

[20] Y.H. He, H. Guo, S. Hwang, X.X. Yang, Z.Z. He, J. Braaten, S. Karakalos, W.T. Shan, M.Y. Wang, H. Zhou, Z.X. Feng, K.L. More, G.F. Wang, D. Su, D.A. Cullen, L. Fei, S. Litster, G. Wu, Single cobalt sites dispersed in hierarchically porous nanofiber networks for durable and high-power PGM-free cathodes in fuel cells, Adv. Mater. 32 (2020) 2003577.

[21] Y.N. Guo, Y. Sugahara, Polymer-derived ceramics for electrocatalytic energy conversion reactions, Int. J. Appl. Ceram. Technol. 20 (2023) 8–23.

[22] P. Moni, M.G. Pollachini, M. Wilhelm, J. Lorenz, C. Harms, M.M. Murshed, K. Rezwan, Metal-containing ceramic composite with in situ grown carbon nanotube as a cathode catalyst for anion exchange membrane fuel cell and rechargeable zinc-air battery, ACS Appl. Energ. Mater. 2 (2019) 6078–6086.

[23] P. Moni, M. Mooste, K. Tammeveski, K. Rezwan, M. Wilhelm, One-dimensional polymer-derived ceramic nanowires with electrocatalytically active metallic silicide tips as cathode catalysts for Zn-air batteries, RSC Adv. 11 (2021) 39707–39717.

[24] S. Abinaya, P. Moni, V. Parthiban, A.K. Sahu, M. Wilhelm, Metal silicide nanosphere decorated carbon-rich polymer-derived ceramics: bifunctional electrocatalysts towards oxygen and their application in anion exchange membrane fuel cells, ChemElectroChem 6 (2019) 3268–3278.

[25] T. Canuto de Almeida e Silva, M. Mooste, E. Kibena-Põldsepp, L. Matisen, M. Merisalu, M. Kook, V. Sammelselg, K. Tammeveski, M. Wilhelm, K. Rezwan, Polymer-derived Co/Ni–SiOC(N) ceramic electrocatalysts for oxygen reduction reaction in fuel cells, Catal. Sci. Technol. 9 (2019) 854–866.

[26] E. Proietti, F. Jaouen, M. Lefèvre, N. Larouche, J. Tian, J. Herranz, J.P. Dodelet, Iron-based cathode catalyst with enhanced power density in polymer electrolyte membrane fuel cells, Nat. Commun. 2 (2011) 416.

[27] Z.X. Song, L. Zhang, K. Doyle-Davis, X.Z. Fu, J.L. Luo, X.L. Sun, Recent Advances in MOF-Derived Single Atom Catalysts for Electrochemical Applications, Adv. Energy Mater. 10 (2020) 2001561.

[28] H.G. Zhang, S. Hwang, M.Y. Wang, Z.X. Feng, S. Karakalos, L.L. Luo, Z. Qiao, X. H. Xie, C.M. Wang, D. Su, Y.Y. Shao, G. Wu, Single atomic iron catalysts for oxygen reduction in acidic media: particle size control and thermal activation, J. Am. Chem. Soc. 139 (2017) 14143–14149.

[29] A. Situ, T.Y. Zhao, Y.T. Huang, P.Z. Li, L.G. Yang, Z.H. Zhang, Z.C. Wang, Y.S. Ou, X.C. Guan, J.X. Wen, J. Zhang, Y.F. Zhan, X.F. Tang, Dual-MOFs-derived Fe and Mn species anchored on bamboo-like carbon nanotubes for efficient oxygen reduction as electrocatalysts, Catalysts 13 (2023) 1161.

[30] J.J. Li, W. Xia, X.T. Xu, D. Jiang, Z.X. Cai, J. Tang, Y.N. Guo, X.L. Huang, T. Wang, J.P. He, B.X. Han, Y. Yamauchi, Selective etching of metal-organic frameworks for open porous structures: mass-efficient catalysts with enhanced oxygen reduction reaction for fuel cells, J. Am. Chem. Soc. 145 (2023) 27262–27272.

[31] R. Kumar, M. Mooste, Z. Ahmed, I. Zekker, M. Käärik, M. Marandi, J. Leis, A. Kikas, M. Otsus, A. Treshchalov, J. Aruväli, M. Jaagura, V. Kisand, A. Tamm, K. Tammeveski, Catalyzing oxygen reduction by morphologically engineered ZIF-derived carbon composite catalysts in dual-chamber microbial fuel cells, J. Environ. Chem. Eng. 12 (2024) 112242.

[32] R. Kumar, M. Mooste, Z. Ahmed, S. Akula, I. Zekker, M. Marandi, M. Käärik, J. Leis, A. Kikas, A. Treshchalov, M. Otsus, J. Aruväli, V. Kisand, A. Tamm, K. Tammeveski, Highly active ZIF-8@CNT composite catalysts as cathode materials for anion exchange membrane fuel cells, Ind. Chem. Mater. 1 (2023) 526–541.

[33] Z. Jiang, X.R. Liu, X.Z. Liu, S. Huang, Y. Liu, Z.C. Yao, Y. Zhang, Q.H. Zhang, L. Gu, L.R. Zheng, L. Li, J.A. Zhang, Y.J. Fan, T. Tang, Z.B. Zhuang, J.S. Hu, Interfacial assembly of binary atomic metal-N_x sites for high-performance energy devices, Nat. Commun. 14 (2023) 1822.

[34] R. Feng, Q.D. Ruan, J.J. Feng, Y.Q. Yao, L.M. Li, L. Zhang, A.J. Wang, Facile pyrolysis synthesis of abundant FeCo dual-single atoms anchored on N-doped carbon nanocages for synergistically boosting oxygen reduction reaction, J. Colloid Interface Sci. 654 (2024) 1240–1250.

[35] I. Palm, R. Sibul, E. Kibena-Põldsepp, M. Mooste, J. Lilloja, M. Käärik, J. Kozlova, A. Kikas, A. Treshchalov, J. Leis, V. Kisand, A. Tamm, N. Bibent, F. Jaouen, S. Holdcroft, K. Tammeveski, ZIF-8 derived iron-, sulphur-, and nitrogen-doped catalysts for anion-exchange membrane fuel cell application, Renew. Energy 228 (2024) 120613.

[36] I. Martinaiou, A. Shahraei, F. Grimm, H. Zhang, C. Wittich, S. Klement, S. J. Dolique, H.J. Kleebe, R.W. Stark, U.I. Kramm, Effect of metal species on the stability of Me-N-C catalysts during accelerated stress tests mimicking the start-up and shut-down conditions, Electrochim. Acta 243 (2017) 183–196.

[37] J.C. Li, Z.Q. Yang, D.M. Tang, L. Zhang, P.X. Hou, S.Y. Zhao, C. Liu, M. Cheng, G. X. Li, F. Zhang, H.M. Cheng, N-doped carbon nanotubes containing a high concentration of single iron atoms for efficient oxygen reduction, NPG Asia Mater. 10 (2018) e461.

[38] P.Q. Yin, T. Yao, Y. Wu, L.R. Zheng, Y. Lin, W. Liu, H.X. Ju, J.F. Zhu, X. Hong, Z. X. Deng, G. Zhou, S.Q. Wei, Y.D. Li, Single cobalt atoms with precise N-coordination as superior oxygen reduction reaction catalysts, Angew. Chem.-Int. Edit. 55 (2016) 10800–10805.

[39] J. Müller-Hülstede, D. Schonvogel, H. Schmies, P. Wagner, A. Dyck, M. Wark, Incorporation of activated biomasses in Fe-N-C catalysts for oxygen reduction reaction with enhanced stability in acidic media, ACS Appl. Energy Mater. 4 (2021) 6912–6922.

[40] J. Hülstede, D. Schonvogel, H. Schmies, P. Wagner, F. Schröter, A. Dyck, M. Wark, Relevant properties of carbon support materials in successful Fe-N-C synthesis for the oxygen reduction reaction: study of carbon blacks and biomass-based carbons, Materials 14 (2021) 45.

[41] K. Muuli, A. Sokka, M. Mooste, J. Lilloja, V. Gudkova, M. Käärik, M. Otsus, A. Kikas, V. Kisand, A. Tamm, A. Krumme, S. Holdcroft, J.H. Zagal, K. Tammeveski, Iron and cobalt phthalocyanine embedded electrospun carbon nanofiber-based catalysts for anion exchange membrane fuel cell cathode, J. Catal. 422 (2023) 117–130.

[42] S. Brunauer, P.H. Emmett, E. Teller, Adsorption of Gases in Multimolecular Layers, J. Am. Chem. Soc. 60 (1938) 309–319.

[43] M. Mooste, E. Kibena-Põldsepp, L. Matisen, M. Merisalu, M. Kook, V. Kisand, V. Vassiljeva, A. Krumme, V. Sammelselg, K. Tammeveski, Oxygen reduction on catalysts prepared by pyrolysis of electrospun styrene-acrylonitrile copolymer and multi-walled carbon nanotube composite fibres, Catal. Lett. 148 (2018) 1815–1826.

[44] T. Zierdt, J. Müller-Hülstede, H. Schmies, D. Schonvogel, P. Wagner, K. A. Friedrich, Effect of polytetrafluorethylene content in Fe-N-C-based catalyst layers of gas diffusion electrodes for HT-PEM fuel cell applications, ChemElectroChem 11 (2024) e202300583.

[45] K. Muuli, R. Kumar, M. Mooste, V. Gudkova, A. Treshchalov, H.M. Piirsoo, A. Kikas, J. Aruväli, V. Kisand, A. Tamm, A. Krumme, P. Moni, M. Wilhelm, K. Tammeveski, Iron, cobalt, and nickel phthalocyanine tri-doped electrospun carbon nanofibre-based catalyst for rechargeable zinc-air battery air electrode, Materials 16 (2023) 4626.

[46] M. Mooste, Z. Ahmed, P. Kapitulskis, R. Ivanov, A. Treshchalov, H.-M. Piirsoo, A. Kikas, V. Kisand, K. Kukli, I. Hussainova, K. Tammeveski, Bifunctional oxygen electrocatalyst based on Fe, Co, and nitrogen co-doped graphene-coated alumina nanofibers for Zn-air battery air electrode, Appl. Surf. Sci. 660 (2024) 160024.

[47] K. Ehelebe, D. Seeberger, M.T.Y. Paul, S. Thiele, K.J.J. Mayrhofer, S. Cherevko, Evaluating electrocatalysts at relevant currents in a half-cell: the impact of Pt loading on oxygen reduction reaction, J. Electrochem. Soc. 166 (2019) F1259–F1268.

[48] L. Ma, R. Wang, Y.H. Li, X.F. Liu, Q.Q. Zhang, X.Y. Dong, S.Q. Zang, Apically Co-nanoparticles-wrapped nitrogen-doped carbon nanotubes from a single-source MOF for efficient oxygen reduction, J. Mater. Chem. A 6 (2018) 24071–24077.

[49] S. Akula, M. Mooste, B. Zulevi, S. McKinney, A. Kikas, H.M. Piirsoo, M. Rahn, A. Tamm, V. Kisand, A. Serov, E.B. Creel, D.A. Cullen, K.C. Neyerlin, H. Wang, M. Odgaard, T. Reshetenko, K. Tammeveski, Mesoporous textured Fe-N-C electrocatalysts as highly efficient cathodes for proton exchange membrane fuel cells, J. Power Sources 520 (2022) 230819.

[50] G.D. Nie, Z.Y. Zhang, T.T. Wang, C. Wang, Z.K. Kou, Electrospun one-dimensional electrocatalysts for oxygen reduction reaction: insights into structure-activity relationship, ACS Appl. Mater. Interfaces 13 (2021) 37961–37978.

[51] M. Primbs, Y.Y. Sun, A. Roy, D. Malko, A. Mehmood, M.T. Sougrati, P. Y. Blanchard, G. Granozzi, T. Kosmala, G. Daniel, P. Atanassov, J. Sharman, C. Durante, A. Kucernak, D. Jones, F. Jaouen, P. Strasser, Establishing reactivity descriptors for platinum group metal (PGM)-free Fe-N-C catalysts for PEM fuel cells, Energy Environ. Sci. 13 (2020) 2480–2500.

[52] H.J. Zhang, X.X. Yuan, L.L. Sun, J.H. Yang, Z.F. Ma, Z.P. Shao, Synthesis and characterization of non-precious metal binary catalyst for oxygen reduction reaction in proton exchange membrane fuel cells, Electrochim. Acta 77 (2012) 324–329.

[53] C.L. Li, M.C. Wu, R. Liu, High-performance bifunctional oxygen electrocatalysts for zinc-air batteries over mesoporous Fe/Co-N-C nanofibers with embedding FeCo alloy nanoparticles, Appl. Catal. B-Environ. 244 (2019) 150–158.

[54] A. Sokka, M. Mooste, M. Käärik, V. Gudkova, J. Kozlova, A. Kikas, V. Kisand, A. Treshchalov, A. Tamm, P. Paiste, J. Aruväli, J. Leis, A. Krumme, S. Holdcroft, S. Cavaliere, F. Jaouen, K. Tammeveski, Iron and cobalt containing electrospun carbon nanofibre-based cathode catalysts for anion exchange membrane fuel cell, Int. J. Hydrog. Energy 46 (2021) 31275–31287.

[55] K. Muuli, M. Mooste, S. Akula, V. Gudkova, M. Otsus, A. Kikas, J. Aruväli, A. Treshchalov, V. Kisand, A. Tamm, A. Krumme, S. Cavaliere, K. Tammeveski, Electrospun carbon nanofibre-based catalysts prepared with Co and Fe phthalocyanine for oxygen reduction in acidic medium, ChemElectroChem 10 (2023) e202300131.

[56] S.S.A. Shah, T. Najam, M.S. Javed, M.M. Rahman, P. Tsiakaras, Novel Mn-/Co-N_x moieties captured in N-doped carbon nanotubes for enhanced oxygen reduction activity and stability in acidic and alkaline media, ACS Appl. Mater. Interfaces 13 (2021) 23191–23200.

[57] X.D. Zhang, X.X. Huang, G.W. Wen, X. Geng, J.D. Zhu, T. Zhang, H.W. Bai, Novel SiOC nanocomposites for high-yield preparation of ultra-large-scale SiC nanowires, Nanotechnology. 21 (2010) 385601.

[58] W.F.A. Besling, A. Goossens, B. Meester, J. Schoonman, Laser-induced chemical vapor deposition of nanostructured silicon carbonitride thin films, J. Appl. Phys. 83 (1998) 544–553.

[59] S. Gallis, V. Nikas, E. Eisenbraun, M.B. Huang, A.E. Kaloyeros, On the effects of thermal treatment on the composition, structure, morphology, and optical properties of hydrogenated amorphous silicon-oxycarbide, J. Mater. Res. 24 (2009) 2561–2573.

[60] N. Yang, X.Y. Zhang, L. Reynolds, D. Kumah, C.Y. Xu, The role of carbon content: a comparison of the nickel particle size and magnetic property of nickel/polysiloxane-derived silicon oxycarbide, Adv. Eng. Mater. 25 (2023) 2201453.

[61] J. Müller-Hülstede, T. Zierdt, H. Schmies, D. Schonvogel, Q. Meyer, C. Zhao, P. Wagner, M. Wark, Implementation of different Fe-N-C catalysts in high temperature proton exchange membrane fuel cells - Effect of catalyst and catalyst layer on performance, J. Power Sources 537 (2022) 231529.

[62] R. Praats, A. Chernyaev, J. Sainio, M. Lundström, I. Kruusenberg, K. Liivand, Supporting critical raw material circularity - upcycling graphite from waste LIBs to Zn-air batteries, Green. Chem. 26 (2024) 2874–2883.

[63] M. Hossen, S. Hasan, R.I. Sardar, J.B. Haider, Mottakin, K. Tammeveski, P. Atanassov, State-of-the-art and developmental trends in platinum group metal-free cathode catalyst for anion exchange membrane fuel cell (AEMFC), Appl. Catal. B-Environ. 325 (2023) 121733.

[64] F. Luo, S. Wagner, W. Ju, M. Primbs, S. Li, H. Wang, U.I. Kramm, P. Strasser, Kinetic Diagnostics and synthetic design of platinum group metal-free electrocatalysts for the oxygen reduction reaction using reactivity maps and site utilization descriptors, J. Am. Chem. Soc. 144 (2022) 13487–13498.

[65] J. Lilloja, E. Kibena-Põldsepp, A. Sarapuu, J.C. Douglin, M. Käärik, J. Kozlova, P. Paiste, A. Kikas, J. Aruväli, J. Leis, V. Sammelselg, D.R. Dekel, K. Tammeveski, Transition-metal- and nitrogen-doped carbide-derived carbon/carbon nanotube composites as cathode catalysts for anion-exchange membrane fuel cells, ACS Catal. 11 (2021) 1920–1931.

[66] J. Lilloja, E. Kibena-Põldsepp, A. Sarapuu, M. Käärik, J. Kozlova, P. Paiste, A. Kikas, A. Treshchalov, J. Leis, A. Tamm, V. Kisand, S. Holdcroft, K. Tammeveski, Transition metal and nitrogen-doped mesoporous carbons as cathode catalysts for anion-exchange membrane fuel cells, Appl. Catal. B Environ. 306 (2022) 121113.

[67] L.C.P. Pérez, N.R. Sahraie, J. Melke, P. Elsässer, D. Teschner, X. Huang, R. Kraehnert, R.J. White, S. Enthaler, P. Strasser, A. Fischer, Polyformamidine-derived non-noble metal electrocatalysts for efficient oxygen reduction reaction, Adv. Funct. Mater. 28 (2018) 1707551.

[68] K.X. Liu, S. Kattel, V. Mao, G.F. Wang, Electrochemical and computational study of oxygen reduction reaction on nonprecious transition metal/nitrogen doped carbon nanofibers in acid medium, J. Phys. Chem. C 120 (2016) 1586–1596.

[69] S. Akula, M. Mooste, J. Kozlova, M. Käärik, A. Treshchalov, A. Kikas, V. Kisand, J. Aruväli, P. Paiste, A. Tamm, J. Leis, K. Tammeveski, Transition metal (Fe, Co, Mn, Cu) containing nitrogen-doped porous carbon as efficient oxygen reduction electrocatalysts for anion exchange membrane fuel cells, Chem. Eng. J. 458 (2023) 141468.

[70] Z.Y. Xiao, P.P. Sun, Z.L. Qiao, K.W. Qiao, H.X. Xu, S.T. Wang, D.P. Cao, Atomically dispersed Fe-Cu dual-site catalysts synergistically boosting oxygen reduction for hydrogen fuel cells, Chem. Eng. J. 446 (2022) 137112.

[71] R. Hao, S. Gu, J. Hu, J.J. Chen, Q.M. Gan, Y.Z. Li, Z.Q. Wang, G.Y. Liu, C.L. Yan, H. M. Yuan, K.Y. Liu, C. Liu, Z.G. Lu, Introducing dual metal centers in high purity pyrrolic-N for superior oxygen reduction reaction, Carbon 209 (2023) 118031.

[72] G. Yusibova, J.M. Assafrei, K.F. Ping, J. Aruväli, P. Paiste, M. Käärik, J. Leis, H. M. Piirsoo, A. Tamm, A. Kikas, V. Kisand, P. Starkov, N. Kongi, Bimetallic metal-organic-framework-derived porous cobalt manganese oxide bifunctional oxygen electrocatalyst, J. Electroanal. Chem. 930 (2023) 117161.

[73] Y. Kumar, S. Akula, J. Kozlova, A. Kikas, J. Aruväli, M. Käärik, A. Treshchalov, J. Leis, V. Kisand, K. Kukli, E. Kibena-Põldsepp, K. Tammeveski, Zinc-assisted synthesis of polymer framework-based atomically dispersed bimetal catalysts for efficient oxygen electrocatalysis in rechargeable zinc-air batteries, J. Energy Storage 86 (2024) 111164.

[74] M.J. Chen, S.M. Peng, M. Sun, S.B. Han, Z.H. Zhou, L.H. Huang, Y.Y. Xu, G. Cheng, L. Yu, Mn^{3+}-rich Manganese Phosphate Targeted for Enhanced Oxygen Reduction Reaction in Zinc-Air Batteries, ChemNanoMat 8 (2022) e202200245.

[75] T. Ghodselahi, M.A. Vesaghi, A. Shafiekhani, A. Baghizadeh, M. Lameii, XPS study of the Cu@Cu_2O core-shell nanoparticles, Appl. Surf. Sci. 255 (2008) 2730–2734.

[76] W.J. Jiang, L. Gu, L. Li, Y. Zhang, X. Zhang, L.J. Zhang, J.Q. Wang, J.S. Hu, Z. D. Wei, L.J. Wan, Understanding the high activity of Fe-N-C electrocatalysts in oxygen reduction: Fe/Fe_3C nanoparticles boost the activity of Fe-N_x, J. Am. Chem. Soc. 138 (2016) 3570–3578.

[77] M.E.M. Buan, A. Cognigni, J.C. Walmsley, N. Muthuswamy, M. Ronning, Active sites for the oxygen reduction reaction in nitrogen-doped carbon nanofibers, Catal. Today 357 (2020) 248–258.

[78] W.J. Fan, Z.L. Li, C.H. You, X. Zong, X.L. Tian, S. Miao, T. Shu, C. Li, S.J. Liao, Binary Fe, Cu-doped bamboo-like carbon nanotubes as efficient catalyst for the oxygen reduction reaction, Nano Energy 37 (2017) 187–194.

[79] S.Y. Zhao, Y. Cheng, J.P. Veder, B. Johannessen, M. Saunders, L.J. Zhang, C. Liu, M.F. Chisholm, R. De Marco, J. Liu, S.Z. Yang, S.P. Jiang, One-pot pyrolysis method to fabricate carbon nanotube supported Ni single-atom catalysts with ultrahigh loading, ACS Appl. Energ. Mater. 1 (2018) 5286–5297.

[80] I.W. Wang, D.A. Kutteri, B.Y. Gao, H.J. Tian, J.L. Hu, Methane pyrolysis for carbon nanotubes and CO_x-Free H_2 over Transition-metal catalysts, Energy Fuels. 33 (2019) 197–205.

[81] Y. Hu, J.O. Jensen, C. Pan, L.N. Cleemann, I. Shypunov, Q.F. Li, Immunity of the Fe-N-C catalysts to electrolyte adsorption: Phosphate but not perchloric anions, Appl. Catal. B-Environ. 234 (2018) 357–364.

[82] R. Kumar, S. Pasupathi, B.G. Pollet, K. Scott, Nafion-stabilised platinum nanoparticles supported on titanium nitride: An efficient and durable electrocatalyst for phosphoric acid based polymer electrolyte fuel cells, Electrochim. Acta 109 (2013) 365–369.

[83] Y. Cheng, M.E. Wang, S.F. Lu, C.J. Tang, X. Wu, J.P. Veder, B. Johannessen, L. Thomsen, J. Zhang, S.Z. Yang, S.Y. Wang, S.P. Jiang, First demonstration of phosphate enhanced atomically dispersed bimetallic FeCu catalysts as Pt-free cathodes for high temperature phosphoric acid doped polybenzimidazole fuel cells, Appl. Catal. B-Environ. 284 (2021) 119717.

[84] X.Y. Xie, L. Shang, X.Y. Xiong, R. Shi, T.R. Zhang, Fe single-atom catalysts on MOF-5 derived carbon for efficient oxygen reduction reaction in proton exchange membrane fuel cells, Adv. Energy Mater. 12 (2022) 2102688.

[85] Y.J. Qiu, J. Yu, W.H. Wu, J. Yin, X.D. Bai, Fe-N/C nanofiber electrocatalysts with improved activity and stability for oxygen reduction in alkaline and acid solutions, J. Solid State Electrochem. 17 (2013) 565–573.

[86] S. Dursun, M.S. Yazici, Mixed carbon-graphene supports for cobalt (II) phthalocyanine as fuel cell cathode, ECS J. Solid State Sci. Technol. 9 (2020) 041008.

[87] M.J. Wu, Q.L. Wei, G.X. Zhang, J.L. Qiao, M.X. Wu, J.H. Zhang, Q.J. Gong, S. H. Sun, Fe/Co double hydroxide/oxide nanoparticles on N-Doped CNTs as highly efficient electrocatalyst for rechargeable liquid and quasi-solid-state zinc-air batteries, Adv. Energy Mater. 8 (2018) 1801836.

[88] Q.Z. Shu, S.X. Yang, X.Y. Zhang, Z.X. Li, Y. Zhang, Y. Tang, H. Gao, C.X. Xia, M. M. Zhao, X.F. Li, H. Zhao, A systematic investigation on the effects of Cu^{2+} contamination on the performances and durability of proton exchange membrane fuel cells, Int. J. Hydrog. Energy 57 (2024) 90–99.

[89] M. Gollasch, J. Müller-Hülstede, H. Schmies, D. Schonvogel, P. Wagner, A. Dyck, M. Wark, Elucidating synergistic effects of different metal ratios in bimetallic Fe/Co-N-C catalysts for oxygen reduction reaction, Catalysts 11 (2021) 841.

[90] X.X. Wang, D.A. Cullen, Y.T. Pan, S. Hwang, M.Y. Wang, Z.X. Feng, J.Y. Wang, M. H. Engelhard, H.G. Zhang, Y.H. He, Y.Y. Shao, D. Su, K.L. More, J.S. Spendelow, G. Wu, Nitrogen-coordinated single cobalt atom catalysts for oxygen reduction in proton exchange membrane fuel cells, Adv. Mater. 30 (2018) 1706758.